J. Serb. Chem. Soc. 91 (0) 1–18 (2026)
JSCS–13789

Original scientific paper
Published 00 MM, 2026

Metal complexes with Schiff base and benzimidazolylphenol ligands with *tert*-butyl and methoxy groups: Structural characterization and biological evaluation

DILDORA PARDAEVA[1], AYDIN TAVMAN[2]*, MAYRAM HACIOGLU[3], ONUR ŞAHIN[4], MEHMET ALTUN[5] and AYŞE SEHER BIRTEKSÖZ TAN[3]

[1]*Istanbul University-Cerrahpaşa, Institute of Graduate Education, Department of Chemistry, 34320, Avcilar, Istanbul, Türkiye,* [2]*Istanbul University-Cerrahpaşa, Faculty of Engineering, Department of Chemistry, Inorganic Chemistry Division, 34320, Avcilar, Istanbul, Türkiye,* [3]*Istanbul University, Faculty of Pharmacy, Department of Pharmaceutical Microbiology, 34452, Beyazit, Istanbul, Türkiye,* [4]*Sinop University, Faculty of Health Sciences, Department of Occupational Health and Safety, 57000 Sinop, Türkiye and* [5]*Istanbul University-Cerrahpaşa, Faculty of Engineering, Department of Chemistry, Organic Chemistry Division, 34320, Avcilar, Istanbul, Türkiye*

(Received 17 February, revised 27 February, accepted 2 June 2026)

Abstract: Two chelating ligands bearing *tert*-butyl and methoxy groups, an ONO type Schiff base ($\mathbf{H_2L^1}$) and a benzimidazolylphenol derivative ($\mathbf{HL^2}$), NO type ligand, and their complexes with $CoCl_2$, $NiCl_2$, $CuCl_2$, $ZnCl_2$ and K_2PdCl_4 (**1a**–**e** and **2a**–**e**, respectively) were synthesized and characterized. Various physicochemical and spectroscopic techniques were used to characterize the ligands. In addition, the crystal structure of $\mathbf{H_2L^1}$ was determined by X-ray diffraction spectroscopy. Keto–enol tautomerism is observed in $\mathbf{H_2L^1}$ according to spectral data. Elemental analysis, molar conductivity, magnetic moment and thermogravimetric analysis, as well as FT-IR, fluorescence, UV–Vis and NMR (for diamagnetic complexes) spectroscopic techniques, were utilized to characterize the complexes. Then, antibacterial, antifungal and antiviral activities of the compound were investigated. Antimicrobial activities of the compounds were tested toward six bacteria and three fungi. Some of the complexes exhibited higher activity towards some microorganisms than the ligands. $\mathbf{HL^2}$ and its complexes were observed to show higher activity compared to $\mathbf{H_2L^1}$ and its complexes, especially against *Staphylococcus aureus*, *Staphylococcus epidermidis* and *Escherichia coli* bacteria, and the fungus *Candida tropicalis*. It was found that **2a** has a potent activity against *S. aureus* and *E. coli*, **2b** against both Gram-positive bacteria (*S. aureus* and *S. epidermidis*) and **2c** against *S. aureus*, *S. epidermidis* and *E. coli* compared to other complexes. Antiviral activity of the compounds was tested against Parainfluenza type-2 virus. In terms of antiviral effect, $\mathbf{H_2L^1}$ showed

* Corresponding author. E-mail: atavman@iuc.edu.tr
https://doi.org/10.2298/JSC260217028P

higher activity than **HL²** and the Co(II) and Cu(II) complexes of **HL²** had the highest activity among the compounds, with rates of 62 and 64 %, respectively.

Keywords: chelating ligand; imine; transition metal complex; antimicrobial; antiviral.

INTRODUCTION

Imine compounds derived from *o*-aminophenols and salicylaldehydes are known as ONO type Schiff bases. Such ligands constitute a class of compounds of considerable interest because of their ability to form chelate structures, as for variety of applications and many interesting properties.[1-4] They form strong chelate complexes due to tridentate characteristics.[5] ONO type Schiff bases are known to exhibit a wide range of biological effects such as antibacterial,[6,7] antifungal,[8,9] anticancer[10–13] and antidiabetic[14] activities. Due to these versatile characteristics, they have significant applications in both industry and biology.

A benzimidazole derivative containing a phenol group is called benzimidazolylphenol. Current and widespread research is being conducted on benzimidazolylphenols, and the results of these studies might be applicable in many areas. In addition, since these compounds have strong fluorescent properties, many studies were published examining photophysical properties along with their complexes.[15–17] We have also conducted various studies on many benzimidazolyl--phenol derivatives and some of their metal complexes, and we reported that these compounds have antimicrobial effects on some bacteria and fungi.[18–21] For example, it was determined that 2-(5-bromo-1*H*-benzimidazol-2-yl)phenol compounds, especially those containing second and even third hydroxyl groups in the phenol ring, have both antioxidant and antibacterial effects considerably higher than others.[22] Cl, Br and NO_2 groups in some 5-methoxy-2-(5-substituted-1*H*-benzimidazol-2-yl)-phenols were observed to increase the antimicrobial activity toward *Staphylococcus aureus*, *Enterococcus faecalis* and *Candida albicans*.[23]

As is known, Cu(II) and Zn(II) ions are essential microelements having important roles in the human body such as enzyme modulators, catalytic and regulatory, oxidative–reductive, *etc*. Cobalt(II), which is a part of vitamin B12, is also an essential metal ion. Various biological activities of some Ni(II) and Pd(II) complexes were also reported.[24,25]

The aim of this study is to prepare a salicylic-based Schiff base and benzimidazolylphenol ligands (**H_2L^1** and **HL²**, Fig. 1) containing *tert*-butyl and methoxy groups and their metal complexes with $CoCl_2$, $NiCl_2$, $CuCl_2$, $ZnCl_2$ and K_2PdCl_4 and to investigate their structural properties and some biological effects. In the context of biological activity, the antibacterial, antifungal and antiviral activities of all compounds were investigated. **H_2L^1** and its various complexes were reported.[26–30] 3d/4f Coordination clusters as cooperative catalysts for diastereoselective Michael addition reactions of Zn_2Y_2 complexes were investigated by Griffiths

et al.[26] Ke *et al.* studied structures and magnetic properties of heterometallic Zn_2Dy_2 tetranuclear clusters.[27,28] Antimicrobial activities of Ni(II) and Ni(II)+ +Zn(II) complexes of $\mathbf{H_2L^1}$ were investigated by Zhao *et al*.[29] Crystallographic insights and biological potency against malaria and oxidative stress of organotin complexes of $\mathbf{H_2L^1}$ were considered.[30] $\mathbf{HL^2}$ derivative of benzimidazolylphenol is commercially available but is being published here for the first time.[31]

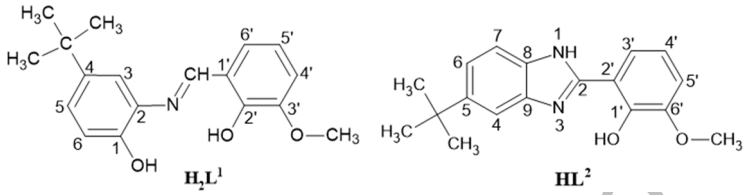

Fig. 1. Chemical structures of the ligands in the study.

EXPERIMENTAL

Chemistry and apparatus

All chemicals and solvents were of reagent grade and they were used without further purification.

The devices and techniques used are as follows. Elemental analysis: LECO combustion analyzer CHNS-932. Melting points: Buchi M-560 melting-point apparatus. Molar conductivity: WTW Cond315i conductivity meter (in DMF at 25 °C). Magnetic measurements: MK1 Sherwood Scientific apparatus (at room temperature by Gouy's method. Diamagnetic corrections were calculated using Pascal's constants). NMR spectroscopy: Varian Unity Inova 500 NMR spectrometer. FT-IR spectroscopy: Perkin Elmer Spectrum Two spectrometer with attenuated total reflection (ATR) techniques, between 400 and 4000 cm^{-1}. The electron spray ionization-mass spectroscopy (ESI-MS positive ion mode): Thermo Finnigan LCQ Advantage MAX LC/MS/MS (in MeOH). Thermogravimetric studies: TG-60WS Shimadzu, between 40 and 700 °C, with a heating rate of 10 °C/min and air flowing at the rate of 50 mL/min. UV–Vis spectra were performed on Shimadzu UV-1800 spectrophotometer in EtOH. Fluorescence spectra: Shimadzu RF-5301 PC spectrofluorophotometer ($c \approx 1\times10^{-4}$ mol/L in EtOH).

Synthesis of the ligands

4-tert-*Butyl-2-{[(*E*)-(2-hydroxy-3-methoxyphenyl)methylidene]amino}phenol* ($\mathbf{H_2L^1}$). 3-methoxysalicylaldehyde (0.78 g, 5 mmol) and 2-amino-4-*tert*-butylphenol (0.825 g, 5 mmol) were dissolved in EtOH (25 mL) and refluxed for 3 h. The crystals formed in the solution that was filtered and kept at room temperature. Red solid. Yield: 77 %.

2-(5-tert-*Butyl-1*H-*benzimidazol-2-yl)-6-methoxyphenol* ($\mathbf{HL^2}$). a modified method developed by us utilizing two different methods available in the literature was applied for synthesis of $\mathbf{HL^2}$.[32-34] 3-Methoxysalicylaldehyde (0.78 g, 5 mmol), 4-*tert*-butylbenzene-1,2-diamine (0.82 g, 5 mmol) and 250 mg H_3BO_3 as catalyst were dissolved in DMF (25 mL) and then this mixture was refluxed for 3 h. After cooling to the room temperature, the reaction mixture was poured into water (250 mL) and then a precipitate was formed. It was filtered, dried and crystallized from ethanol after. Light yellow solid. Yield: 81 %.

Preparation of the complexes

Appropriate metal salt solutions (1 mmol of $CoCl_2 \cdot 6H_2O$, $NiCl_2 \cdot 6H_2O$, $ZnCl_2 \cdot 6H_2O$ in 10 mL of ethylacetate; $CuCl_2 \cdot 2H_2O$ in 10 mL methanol, K_2PdCl_4 (was obtained by dissolving 1 mmol $PdCl_2$ (0.177 g) and 2 mmol KCl (0.15 g) in 10 mL MeOH+H_2O mixture (6:4 volume ratio))) were added gradually to the solutions of the ligands (1 mmol, *i.e.*, ~300 mg of $\mathbf{H_2L^1}$) in appropriate solvent (10 mL) and heated for 3 h under reflux. Cu(II) and Pd(II) salts gave immediately precipitates with the ligands. The other complex solutions were kept at room temperature; precipitates formed within a few days. The precipitates were filtered off, washed with distilled water and kept at room temperature to dry.

Analytical and spectral data of the synthesized ligands, and complexes **1a**–**e** and **2a**–**e** compounds are given in the Supplementary material to this paper.

Determination of antibacterial and antifungal activity

Antimicrobial activities of the compounds were investigated against standard ATCC strains of bacteria and fungi by the microbroth dilutions way according to the Clinical and Laboratory Standards Institute (CLSI) guidance.[35,36] The antimicrobial activity procedure and the microorganisms used are the same as in our previous studies.[8,9] The experiments were carried out in duplicate.

Antiviral activity assay

For Parainfluenza Type-2 virus (PIV-2), African green monkey kidney cell line (VERO, ATCC) was cultured in Dulbecco's modified Eagle's medium (Wisent, Multicell) supplemented with 10 % fetal bovine serum (FBS; Sigma), 100 U/mL penicillin and 100 μg/mL streptomycin. The PIV-2 and cells were maintained at 37 °C under 5 % CO_2 atmosphere. An experiment was conducted based on the plaque formation test for PIV-2 strain that grown on VERO cell culture.[37] VERO cells were infected with PIV-2 at 100 PFU per well, one of the wells was used as a control and the antiviral activities of the samples were tested in the other wells. The virus--infected control (ribavirin) well was accepted as 100 %, and the efficacy results were calculated as a percentage by comparing this control value. The concentration of the compounds is 10 mg/mL.

X-ray single crystal diffraction analysis

$\mathbf{H_2L^1}$ was crystallized from EtOH. The red colored single crystals were obtained. Suitable crystals were selected for data collection which was performed on a Bruker-D8 QUEST diffractometer equipped with a graphite-monochromatic Mo-K_α radiation at 296 K. The structure of $\mathbf{H_2L_1}$ was solved by direct methods using SHELXS-2013[38] and refined by full-matrix least--squares methods on F^2 using SHELXL-2013.[39] All non-hydrogen atoms were refined with anisotropic parameters. The H atoms of C atoms were located from different maps and then treated as riding atoms with C–H distance of 0.93–0.97 Å. The other H atoms were located in a difference map refined freely. The following procedures were implemented in our analysis. Data collection: Bruker APEX2;[40] program used for molecular graphics were as follow: Mercury programs;[41] software used to prepare material for publication: WinGX.[42] Details of data collection and crystal structure determinations are given in Table S-I of the Supplementary material. Crystallographic data for the structural analysis are deposited with the Cambridge Crystallographic Data Centre, CCDC No. 2298000.

RESULTS AND DISCUSSION

Crystal structure of H_2L^1

Crystal data and structure refinement and hydrogen bond parameters related $\mathbf{H_2L^1}$ are given in Tables S-I and I, respectively. Selected bond distances and angles are given in Table S-II of the Supplementary material. Molecular structure of $\mathbf{H_2L^1}$ is shown in Fig. 2.

TABLE I. Hydrogen bonding parameters for $\mathbf{H_2L^1}$; symmetry code: (*i*) −*x*+1/2, *y*+1/2, *z*

D–H···A	D–H, Å	H···A, Å	D···A, Å	D–H···A, °
N1–H1···O1	0.88(2)	1.88(2)	2.598(2)	138(2)
O3–H3*A*···O1^{i}	0.83(2)	1.83(2)	2.657(2)	178(3)

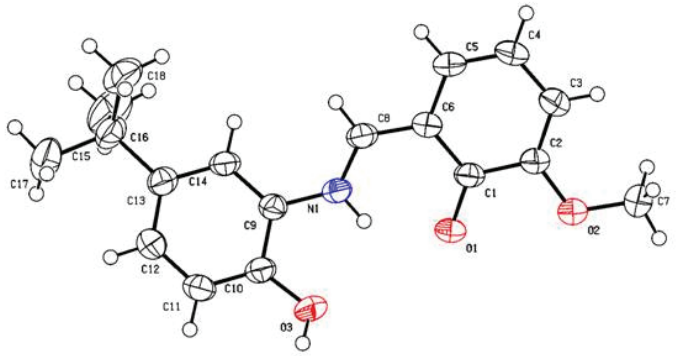

Fig. 2. Molecular structure of $\mathbf{H_2L^1}$ showing the atom numbering scheme.

From the X-ray data, it appears that the keto structure is valid for $\mathbf{H_2L^1}$ in solid state as stated in our previous studies.[2,9] In the crystal structure of $\mathbf{H_2L^1}$, the C–O bond length in the 2-hydroxy-3-methoxyphenyl part is shorter than the other (4-*tert*-butyl-2-hydroxyphenylimino part, 1.289(2) and 1.353(3) Å, respectively). This difference between the C–O bond lengths is due to the keto structure being more dominant than the enol structure.

General properties

$\mathbf{H_2L^1}$, an ONO type imine compound, is a dibasic and tridentate chelating ligand whereas $\mathbf{HL^2}$ is a monobasic bidentate chelating NO type ligand. ESI-MS data showing formation of the ligands are given in the experimental section, and the spectra are given in the Supplementary material (Figs. S-1 and S-2). Both ligands appear to tend to form 1:1 complexes, which is probably due to the steric effect of the substituents. It was also expected that $\mathbf{HL^2}$, which is a bidentate ligand, would give a 1:2 complex, but the steric effect of the substituents and the

character of the metal salt (chloride salts) can be considered factors that favor the 1:1 formation.

The magnetic moment values of the Ni(II) complexes were found to be 2.04 and 2.05 BM for $\mathbf{H_2L^1}$ and $\mathbf{HL^2}$ complexes, respectively. These values are lower than the 2.83 BM expected for octahedral or tetrahedral geometries, which are paramagnetic structures that the d^8 ion with two unpaired electrons may have. Such low values are generally thought to be due to the distorted geometry between the tetrahedral and square planar systems, called quasi-tetrahedral.[43–45] Co(II) complex of $\mathbf{H_2L^1}$ (**1a**) has a magnetic moment of 4.06 BM according to the measurements. It was reported that geometry of Co(II) complexes, having magnetic moment values below 4.70 BM, is trigonal bipyramide or square pyramidal (penta-coordinated).[46] According to this finding, the geometry of **1a** may be regarded as square pyramidal in a high-spin structure (three unpaired electrons). The magnetic moment value of Cu(II) complex of $\mathbf{H_2L^1}$ (**1c**) at room temperature was found to be 1.72 BM, indicating formation of a monomeric Cu(II) complex. This value is very close to the theoretical value of 1.71 BM for the d^9 electron configuration. The Cu(II) complex of $\mathbf{HL^2}$ (**2c**) was found to be 1.01 BM, which indicates a Cu(II)–Cu(II) interaction. It suggests that a dimeric structure with a chloride bridge is formed in this complex and thus the Cu(II)–Cu(II) interaction occurs.

The magnetic moment value of the Co(II) complex of $\mathbf{HL^2}$ (**2a**) was measured as 2.17 BM. This value indicates a structure with 1 and 2 unpaired electrons, which may result from a chloride-bridged structure or five-coordination geometry showing M–M interaction for the Co(II) ion with the d^7 structure.[47]

The molar conductivity values of the complexes, except for the Pd(II) complex of $\mathbf{H_2L^1}$ (**1e**) in DMF, were measured to be below 50 Ω^{-1} cm^2 mol^{-1}. According to Geary, compounds with a molar conductivity below 50 Ω^{-1} cm^2 mol^{-1} are considered non-ionic or non-electrolyte.[48] It can be concluded that the Pd(II) complex of $\mathbf{H_2L^1}$, which has a molar conductivity value of 83.2 Ω^{-1} cm^2 mol^{-1}, is 1:1 electrolyte. This result, which is also supported by the elemental analysis values, shows that the K[Pd($\mathbf{L^1}$)Cl] structure is possible.[8]

NMR spectra

NMR spectral data and their assignments of the ligands and the diamagnetic complexes are given in the Supplementary material. ^{1}H- and ^{13}C-NMR spectra of the compounds are given in Figs. S-3–S-14.

There is significant information for structural characterization of Schiff base $\mathbf{H_2L^1}$ having two hydroxyl groups (salicylic and phenolic OHs) in the ^{1}H-NMR. The signals at 9.57 and 9.00 ppm should belong to phenolic OH and N=CH protons, respectively.[10] Salicylic OH proton, on the other hand, was dissociated due to its high acidic character and its signal could not be detected by the device. As a result, it can be asserted that the keto state of $\mathbf{H_2L^1}$ is dominant in the solid state

while the enol state is dominant in the solution (Fig. 3). According to the crystal structure analysis, $\mathbf{H_2L^1}$ has a keto structure in the solid state.

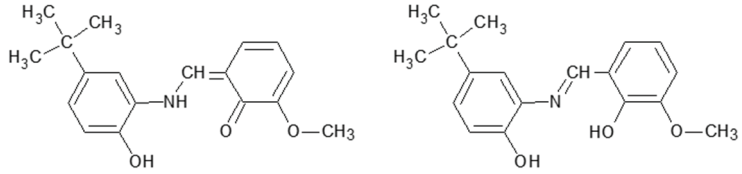

Fig. 3. Structure of $\mathbf{H_2L^1}$ in solid state (keto form, left) and solution with polar solvents (enol form, right).

Phenolic protons of the ligands are not observed in the ^{1}H-NMR spectra of the Pd(II) and Zn(II) complexes, since they removed along with the complex formation. In addition, the azomethine proton (–N=CH–) of the Schiff base ligand shifted considerably to the lower frequency (upfield) on complexation. For example, N=CH proton shows shifting with 0.36 ppm (from 9.00 to 8.64 ppm) in the Pd(II) complex of $\mathbf{H_2L^1}$. It appeared at 8.86 ppm in the Zn(II) complex.

The signal at 161.6 ppm in the ^{13}C-NMR spectra of $\mathbf{H_2L^1}$ should be due to azomethine carbon atom in enol form of the imine compound. The signals of the carbon atoms bonded to the oxygen atom (C1, C2' and C3') of $\mathbf{H_2L^1}$ are detected at the 148.6–152.5 ppm range. In the Pd(II) complex, the azomethine carbon shifted to 174.3 ppm, while the carbon atoms to which the oxygen atoms are bonded were found between 161.5 and 146.9 ppm. In the Zn(II) complex, the N=CH carbon was detected at 164.8 ppm, while the carbon atoms bonded to oxygen were detected between 161.3 and 144.8 ppm.

In $\mathbf{HL^2}$, the NH and OH protons gave a single broad band at 13.12 ppm (integral value = 2H). The broad signals corresponding to a single proton seen at 13.64 and 13.22 ppm in the Zn(II) and Pd(II) complexes, respectively, should belong to the NH proton. The disappearance of the signal belonging to the OH proton indicates that this proton was removed with the complexation of the phenolic oxygen. Sufficient data could not be obtained from ^{13}C-NMR analyses of complexes of $\mathbf{HL^2}$.

IR spectra

The major IR spectral data are presented in the Supplementary material. FTIR spectra of the compounds are given as supplementary material (Figs. S-15–S-26). The IR spectra of the Schiff base ($\mathbf{H_2L^1}$) and its complexes show medium intensity absorption bands at 1630–1647 cm^{-1} assigned to the ν(C=N). The C=N stretching mode of the benzimidazolylphenol derivative ($\mathbf{HL^2}$) and its complexes are observed at the 1602–1619 cm^{-1} range. The medium bands seen between 1576 and 1619 cm^{-1} can be attributed to the C=C stretching mode of the ring systems, which is expected to appear around 1600 cm^{-1}. On complexation, considerable changes

such as a shift to a higher wavenumber and a decrease in the intensity of absorptions were observed in the C=N band characteristic. These changes may support the argument of the imine nitrogen atom coordination in the complexes of both Schiff base and benzimidazolylphenol ligands.

The strong bands at the 1182–1258 cm^{-1} range are attributed to the C–O stretching vibrations of the ligands and the complexes.[49,50]

In the spectra of all the compounds, generally weak bands appearing between 3054 and 3080 cm^{-1} can be attributed to stretching vibration of aromatic CH; strong or medium intensity bands detected in the range of 812–831 cm^{-1} can be interpreted as originating from the bending modes of aromatic CH groups.[51]

As a difference from the ligands, the new broad medium or weak bands between 667 and 688 cm^{-1} in the IR spectra of the complexes, can be attributed to ν(M←N) coordination band (Fig. 4).[22]

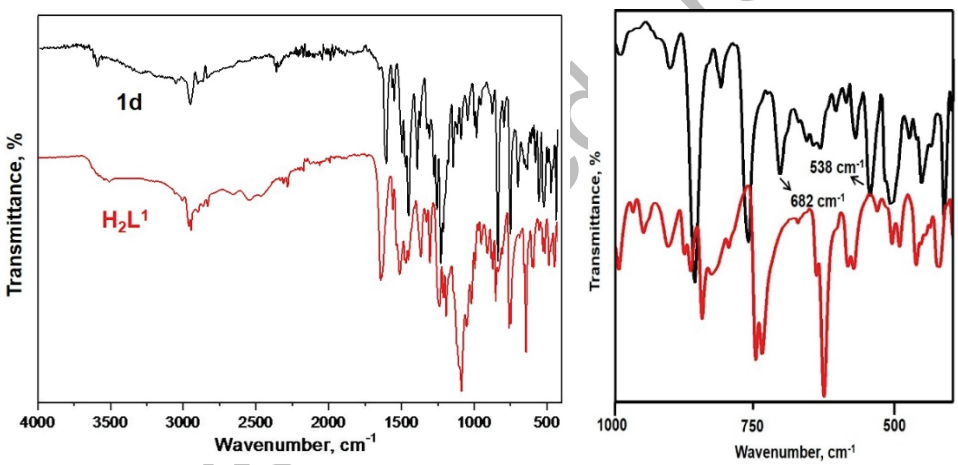

(a) (b)

Fig. 4. Infrared spectra of $\mathbf{H_2L^1}$ (a) and its Zn(II) complex (b), **1d**.

New medium bands at lower frequency at the 536–545 cm^{-1} range in the complexes may be assigned to ν(M←OC) vibration frequencies and this finding can be considered as supporting information for the phenolic oxygen atom coordination (Fig. 4).[52]

UV–Vis spectra

The UV–Vis absorption spectra were obtained in dimethylsulfoxide (DMSO) at room temperature. Experimental maximum absorption wavelength data of the compounds are presented in the Supplementary material. UV–Vis spectra of the compounds are given in the Supplementary material (Figs. S-27–S-38). The bands between 300 and 350 nm involve π→π* transitions whereas the bands at the range

of 350–400 nm can be attributed to n→π* transitions. The band at 456 nm in **H_2L^1** is associated with intramolecular charge transfer transitions.[53]

The absorptions at 451 and 458 nm in the Pd(II) complexes of **H_2L^1** and **HL^2**, respectively, can be assigned to d–d transitions and indicate square planar stereochemistry in solution and can be assigned to $^1A_{1g}\rightarrow{}^1A_{2g}$ transition.[9] The weak bands appearing in the visible region can be attributed to d–d transitions. For example, the bands in the range of 433–478 nm in **1b**, **1c**, **2b** and **2c** (Ni(II) and Cu(II) complexes), can be associated with the $^4A_2\rightarrow{}^4T_1(P)$ (ν_3) transition arising from a tetrahedral geometric structure.[42] The 464 and 473 nm transitions observed in Co(II) complexes, for **1a** and **2a**, respectively, can be attributed to the $^3B(F)\rightarrow$ $\rightarrow{}^3E(P)$ transitions in the square pyramidal structure in solution environment.[54,55] Since there are no allowed d–d transitions in Zn(II) complexes (**1d** and **2d**), the bands at the 350–465 nm range probably originate from the intra-ligand and metal--to-ligand charge transfer transitions.

Fluorescence spectra

Fluorescence spectroscopy measurements of **HL^2**, a benzimidazolylphenol derivative, and its complexes were carried out. Fluorescence spectral data of the compounds, obtained at a concentration of approximately 1×10^{-4} mol/L in ethanol at room temperature, are given in experimental section (excitation wavelength: 354 nm). The fluorescence spectra of **HL^2** and its complexes are given in Fig. 5.

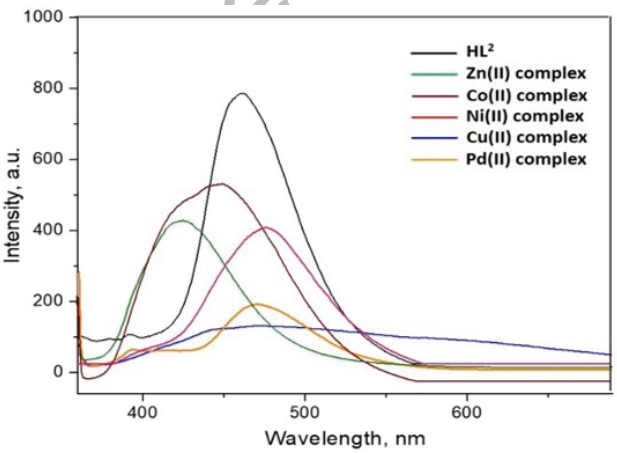

Fig. 5. Comparative fluorescence spectra of **HL^2** and its complexes.

HL^2 emit at 463 nm strongly. In the complexes, the emission values vary between 425 and 478 nm and the intensity decreases. In Co(II), Cu(II) and Zn(II) complexes, emission is observed at a lower wavelength (blue shift) relative to the ligand, while in Ni(II) and Pd(II) complexes, it is observed at a higher wavelength

(red shift). The common feature of the last two metal ions is that they both have the d^8 electronic configuration system. The fluorescence intensity decreases significantly in Pd(II) and Cu(II) complexes. This effect is particularly pronounced in the Cu(II) complex. This indicates that the Cu(II) ion quenches the fluorescence property of the ligand (quenching effect).

Thermogravimetric analysis

The weight loss data obtained from thermal analysis studies are outlined in the Supplementary material. The samples were heated from room temperature up to 700 °C in air atmosphere. Thermogravimetric analysis (TGA) curves of complexes provide important clues for explaining the thermal behavior of molecules and especially the state of water molecules. It is known that lattice H_2O molecules remove from the complex below 100 °C and coordinate H_2O molecules up to 200 °C. Approximately 9.5 and 12.3 % mass losses observed in TGA curves of Co(II) and Ni(II) complexes of $\mathbf{H_2L^1}$ (**1a** and **b**, respectively), below 200 °C can be considered as an indication of presence of two moles of coordinated water molecules (Fig. 6). This valuation is reasonable, considering that two moles of H_2O in the complexes correspond to theoretical masses of 8.8 and 9.2 %, respectively. The mass losses of 3.6 to 4.5 % observed in compounds **1a**, **1d**, **1e**, **2b** and **2d** below 100 °C indicate the presence of one mole of lattice water in these compounds (the theoretical values for these complexes are in the 3.6–4.5 % range). TGA curves of **2a**–**e** are given in the Supplementary material as Figs. S-39–S-43.

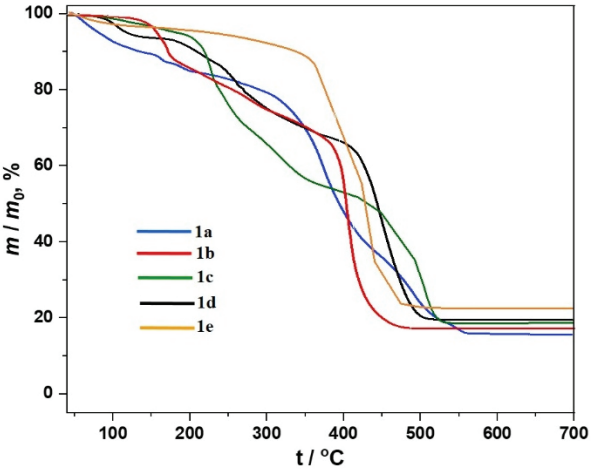

Fig. 6. TGA curves of the complexes **1a**–**e**.

It was observed that the complexes began to decompose above 300 °C and are completely decomposed above 500 °C, forming metal oxide forms. The mass

ratios remaining from the complexes after complete decomposition are consistent with the theoretical mass ratios calculated for metal oxides.

Various complexes of $\mathbf{H_2L^1}$ were reported in the literature. Griffiths *et al.* reported the synthesis and crystal structure of heterobimetallic 3d/4f coordination cluster formulated as $[Zn_2Y_2(\mathbf{L^1})_4(NO_3)_2(DMF)_2]$ and study of its catalytic properties toward the Michael addition of nitrostyrenes with barbituric acid derivatives.[26] Effect of alcoholic solvent and acetate anion coordination mode variations on structures and magnetic properties of heterometallic Zn_2Dy_2 tetranuclear clusters was studied.[27,28] Zhao *et al.* reported tetranuclear complexes of $\mathbf{H_2L^1}$, $[Ni_4(\mathbf{L^1})_4(CH_3OH)_4]$ and $[Ni_2Zn_2Cl_2(\mathbf{L^1})_2(\mu_{1,1}\text{-}N_3)_2]\cdot H_2O$, and investigated their antimicrobial activities.[29] All of these complexes have a tetranuclear structure. Some mononuclear diorganotin(V) complexes of $\mathbf{H_2L^1}$, $R_2Sn\mathbf{L^1}$ (R = Me, Et, Bu, Ph), were obtained and their antimalarial and antioxidant activities were investigated by Taxak *et al*.[30]

Factors such as the crystallization method, the kind of metal salt and the solvent used, are significant in complex formation. In our study, we used chloride salts of metals and attempted to obtain single crystals using various solvents, but we were unsuccessful. Therefore, we do not have evidence to suggest whether our complexes are mononuclear or polynuclear. It is also possible that some of our complexes are polynuclear or as in the literature. Consequently, in the light of the analytical and spectroscopic data obtained, the tentatively proposed structures in Fig. 7 can be suggested for the complexes in the study.

Antimicrobial activity

In vitro antimicrobial activity test results of the ligands ($\mathbf{H_2L^1}$ and $\mathbf{HL^2}$) and their metal complexes in terms of *MIC* are presented in Table III in comparison with the values of the antibiotics and antifungal agents.

Table III shows that the benzimidazole derivative ($\mathbf{HL^2}$) exhibits a higher antimicrobial effect compared to the Schiff base ($\mathbf{H_2L^1}$), particularly against *Staphylococcus epidermidis* (a Gram-positive bacteria) and *Candida tropicalis* (a fungi). On the other hand, it appears that the Co(II) complex of $\mathbf{HL^2}$ (**2a**) has a high activity against *Staphylococcus aureus* and *Escherichia coli*, the Ni(II) complex (**2b**) against both Gram-positive bacteria (*S. aureus* and *S. epidermidis*), and the Cu(II) complex (**2c**) against *S. aureus*, *S. epidermidis* and *E. coli* compared to other complexes. Another noteworthy finding of the study was that **1a**, **1c**, **1d** and **1e** showed significantly higher activity against *C. tropicalis* compared to the ligand.

In the literature, the antimicrobial activities of $\mathbf{H_2L^1}$ and its tetranuclear Ni(II) complex were investigated by Zhao *et al.* against *S. aureus* and *E. coli* bacterial strains, which are also included in the bacterial groups that we studied.[29] They reported antimicrobial activities for $\mathbf{H_2L^1}$ of 75 μM (*S. aureus*) and 37.5 μM (*E. coli*), which differ greatly from our results (625 μg/mL for both bacterial strains).

There could be several reasons for such significantly different results in the studies. First, there is a difference in methods: the literature uses a colorimetric method using dye 3-(4,5-dimethylthiazol-2-yl)-2,5-diphenyltetrazolium bromide (MTT) published in 2000.[56] Our method is a relatively new published by CLSI in 2021.[36] In addition, factors such as user errors and the chemicals used (DMSO, culture medium, *etc*.) may also be influential. The reproducibility of the experiment is also important. Our experiments were repeated twice. The number of repetitions in the literature is not specified. Therefore, the difference in results can be considered reasonable.

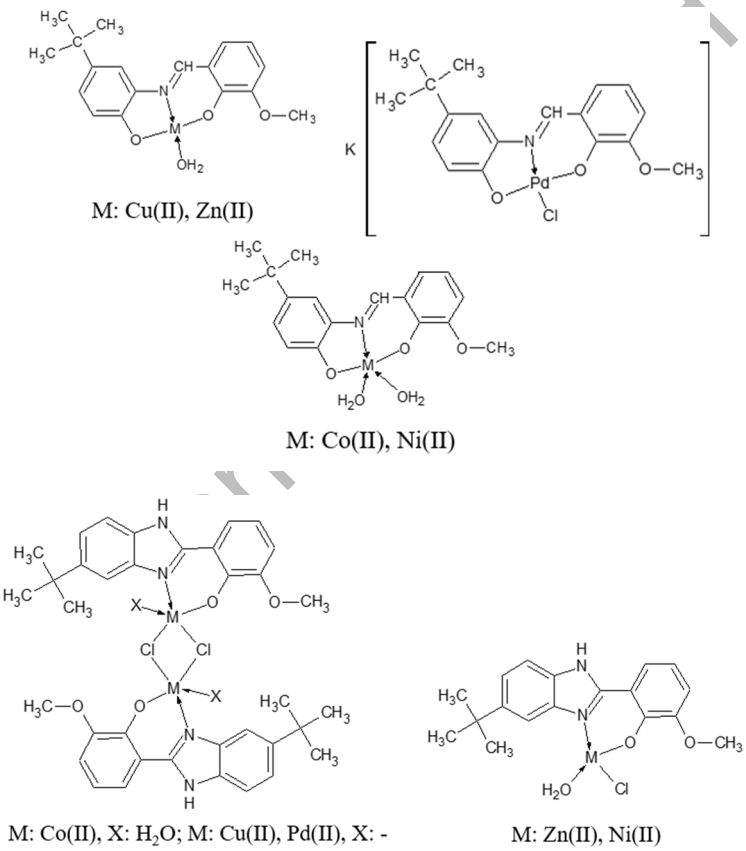

Fig. 7. Tentatively proposed structures for the complexes in the study.

Antiviral activity

Antiviral activity of the compounds was tested against Parainfluenza type-2 virus and the results are given at Table IV as percent inhibition. It was found that while $\mathbf{H_2L^1}$ inhibited viruses by 51 %, $\mathbf{HL^2}$ was found to be effective with a rate

385 of 26 %. Accordingly, it appears that Schiff base, $\mathbf{H_2L^1}$, has the antiviral effect
386 approximately twice higher than the benzimidazole compound, *i.e.*, $\mathbf{HL^2}$.

387 TABLE III. *In vitro* antimicrobial activity of the compounds (*MIC* / μg mL^{-1}); *Sa – Staphylo-*
388 *coccus aureus* ATCC 6538; *Se – Staphylococcus epidermidis* ATCC 12228; *Ec – Escherichia*
389 *coli* ATCC 8739; *Kp – Klebsiella pneumoniae* ATCC 4352; *Pa – Pseudomonas aeruginosa*
390 ATCC 1539; *Pm – Proteus mirabilis* ATCC 14153; *Ca – Candida albicans* ATCC 10231; *Cp*
391 *– Candida parapsilosis* ATCC 22019; *Ct – Candida tropicalis* ATCC 750; [a]Gram-positive;
392 [b]Gram-negative; –: no antimicrobial effect at 5000 μg/mL and lower dilutions; ciprofloxacin
393 and amphotericin B were used as references for bacteria and fungi, respectively

Compound	Microorganism								
	Sa	*Se*[a]	*Ec*[b]	*Kp*[b]	*Pa*[b]	*Pm*[b]	*Ca*	*Cp*	*Ct*
$\mathbf{H_2L^1}$	625	625	625	625	312	625	312	156	625
1a	312	312	625	625	625	625	312	–	156
1b	625	625	1250	625	–	625	1250	1250	312
1c	625	625	1250	1250	625	1250	625	625	156
1d	1250	156	1250	312	1250	625	1250	625	156
1e	312	625	312	625	625	625	312	156	156
$\mathbf{HL^2}$	625	156	312	–	625	625	–	1250	156
2a	78	156	78	156	312	312	312	625	156
2b	**19.5**	**39**	156	625	625	–	–	625	–
2c	78	**19.5**	78	312	625	–	625	625	312
2d	312	312	156	626	625	312	312	625	312
2e	312	312	312	312	625	–	–	312	–
Reference	0.25	0.25	0.007	0.007	0.125	0.007	0.5	1.0	1.0

394 In all complexes of $\mathbf{HL^2}$, the antiviral effect significantly increased compared
395 to the ligand. It is particularly interesting that **2a** and **2c** showed virus inhibition
396 effect at the rates 62 and 64 %, respectively.

397 TABLE IV. Antiviral activity of the compounds; ribavirin: reference antiviral agent

Compound	Virus Inhibition, %
$\mathbf{H_2L^1}$	51
1a	37
1b	29
1c	34
1d	33
1e	42
$\mathbf{HL^2}$	26
2a	62
2b	52
2c	64
2d	43
2e	35
Ribavirin	100

This study is limited to one Schiff base containing *tert*-butyl and methoxy groups, one benzimidazolylphenol ligand and five complexes of each. More comprehensive studies can be conducted using a larger number of similar ligands and different complexes. For example, it might be interesting to investigate how would the activities of compounds, obtained by substituting the methoxy groups (*e.g.*, 4- or 5-substituted), change. Changes in activity can be observed by forming complexes with different metal ions such as Mn(II), Fe(III), Ag(I) and VO(II). One of the advantages of our study is that the activity against a wide range of bacteria and fungi has been investigated. Another advantage is that the antiviral effect has been investigated, and studies on the antiviral activity of such compounds are quite limited.

CONCLUSION

This study deals with two chelating ligands containing *tert*-butyl and methoxy groups in their structures, an ONO-type Schiff base ($\mathbf{H_2L^1}$) and benzimidazolylpenol ($\mathbf{HL^2}$), an NO-type ligand, and their various transition metal complexes (**1a**–**e**, **2a**–**e**) and their various biological properties. A study group consisting of a total of 12 compound samples was formed by obtaining Co(II), Ni(II), Cu(II), Zn(II) and Pd(II) complexes of both ligands.

The structure of $\mathbf{H_2L^1}$ was investigated using single crystal X-ray diffraction spectroscopy. There is keto-enol tautomerism in $\mathbf{H_2L^1}$ according to spectral data. All the compounds were characterized using physicochemical and spectroscopic methods such as elemental analysis, FT-IR, UV–Vis and NMR spectroscopic techniques. Molar conductivity and magnetic moment measurements and thermogravimetric analysis were applied the complexes also. Fluorescence spectroscopy was performed on $\mathbf{HL^2}$ and its complexes due to their fluorescence properties.

In terms of biological applications, antibacterial, antifungal, and antiviral tests were performed on all compounds toward six bacteria, three fungi and Parainfluenza type-2 virus. Generally, $\mathbf{HL^2}$ and its complexes showed higher activity compared to $\mathbf{H_2L^1}$ and its complexes, especially on *S. aureus*, *S. epidermidis* and *E. coli* bacteria, and the fungus *C. tropicalis*. Some of the complexes, such as **1a** and **b**, and all complexes of $\mathbf{HL^2}$, exhibited higher activity than the ligands against many bacteria and *C. tropicalis*. In the comparison between the complexes, it was observed that **2a**, **b** and **c** showed higher antibacterial activity, especially against *S. aureus*, *S. epidermidis* and *E. coli*, compared to the others. Regarding antiviral activity, $\mathbf{H_2L^1}$ showed higher activity than $\mathbf{HL^2}$ on Parainfluenza type-2 virus. However, Co(II) and Cu(II) complexes of $\mathbf{HL^2}$ (**2a** and **c**) were observed to have the highest activity among the compounds, with rates of 62 and 64 %, respectively.

SUPPLEMENTARY MATERIAL

Additional data and information are available electronically at the pages of journal website: https://www.shd-pub.org.rs/index.php/JSCS/article/view/13789, or from the corresponding author on request.

Acknowledgements. This work was supported by Scientific Research Projects Coordination Unit of Istanbul University-Cerrahpasa (Project number: 36370) and The Scientific and Technological Research Council of Türkiye (TUBITAK, Project number: 123Z795).

ИЗВОД

КОМПЛЕКСИ МЕТАЛА СА ШИФОВИМ БАЗАМА И БЕНЗИМИДАЗОЛИЛФЕНОЛНИМ ЛИГАНДИМА СА *ТЕРЦ*-БУТИЛ И МЕТОКСИ ГРУПАМА: СТРУКТУРНА КАРАКТЕРИЗАЦИЈА И БИОЛОШКО ИСПИТИВАЊЕ

DILDORA PARDAEVA[1], AYDIN TAVMAN[2], MAYRAM HACIOGLU[3], ONUR ŞAHIN[4], MEHMET ALTUN[5] и A. SEHER BIRTEKSÖZ TAN[3]

[1]Istanbul University-Cerrahpaşa, Institute of Graduate Education, Department of Chemistry, 34320, Avcilar, Istanbul, Türkiye, [2]Istanbul University-Cerrahpaşa, Faculty of Engineering, Department of Chemistry, Inorganic Chemistry Division, 34320, Avcilar, Istanbul, Türkiye, [3]Istanbul University, Faculty of Pharmacy, Department of Pharmaceutical Microbiology, 34452, Beyazit, Istanbul, Türkiye, [4]Sinop University, Faculty of Health Sciences, Department of Occupational Health and Safety, 57000 Sinop, Türkiye и [5]Istanbul University-Cerrahpaşa, Faculty of Engineering, Department of Chemistry, Organic Chemistry Division, 34320, Avcilar, Istanbul, Türkiye

Синтетисана су и окарактерисана два хелатна лиганда са *терц*-бутил и метокси групама, Шифова база ONO типа (**H_2L^1**) и бензимидазолилфенолни дериват (**HL^2**), лиганд NO типа, као и њихови комплекси у реакцијама са $CoCl_2$, $NiCl_2$, $CuCl_2$, $ZnCl_2$ и K_2PdCl_4 (**1a**–**e**, **2a**–**e**). За карактеризацију лиганада коришћене су различите физичкохемијске и спектроскопске технике. Поред тога, кристална структура **H_2L^1** лиганда одређена је рендгенском структурном анализом. На основу спектроскопских података за **H_2L^1** примећена је појава кето–енолне таутомерије. За карактеризацију комплекса коришћене су елементална анализа, моларна проводљивост, магнетна мерења, термогравиметријска анализа, FT-IR, флуоресцентна, UV–Vis и NMR спектроскопија (за дијамагнетнетне комплексе). Испитиване су антибактеријска, антигљивична и антивирусна активност синтетисаних једињења. Антимикробна активност једињења је испитивана према шест бактеријских и три гљивичне врсте. Неки од комплекса су показали већу активност према појединим микроорганизмима у односу на лиганде. Уочено је да **HL^2** лиганд и његови комплекси показују већу активност у поређењу са **H_2L^1** и његовим комплексима, нарочито према бактеријама *Staphylococcus aureus, Staphylococcus epidermidis* и *Escherichia coli*, као и према гљивици *Candida tropicalis*. Утврђено је да **2a** показује изражену активност према *S. aureus* и *E. coli*, **2b** према обе Грам-позитивне бактерије (*S. aureus* и *S. epidermidis*), а **2c** према *S. aureus*, *S. epidermidis* и *E. coli* у поређењу са осталим комплексима. Антивирусна активност једињења испитивана је према вирусу параинфлуенце тип-2. У погледу антивирусног ефекта, **H_2L^1** је показао већу активност од **HL^2**, док су кобалт(II) и бакар(II) комплекси **HL^2** лиганда показали највећу активност међу свим једињењима, са процентима инхибиције од 62 и 64 %, редом.

(Примљено 17. фебруара, ревидирано 27. фебруара, прихваћено 2. јуна 2026)

REFERENCES

1. A. Çinarli, D. Gürbüz, A. Tavman, A. S. Birteksöz, *Chinese J. Chem.* **30** (2012) 449 (https://doi.org/10.1002/cjoc.201180473)
2. D. Gürbüz, A. Çinarli, A. Tavman, A. S. Birteksöz, *Chinese J. Chem.* **30** (2012) 970 (https://doi.org/10.1002/cjoc.201100237)

3. B. S. Kusmariya, A. P. Mishra, *J. Mol. Struct.* **1130** (2017) 727. (https://doi.org/10.1016/j.molstruc.2016.11.009)
4. D. Gürbüz, A. Çinarli, A. Tavman, A. S. B. Tan, *Bull. Chem. Soc. Ethiop.* 29 (2015) 63 (https://doi.org/10.4314/bcse.v29i1.6)
5. E. Alterhoni, A. Tavman, D. Gürbüz, M. Hacioglu, A. Çinarli, O. Şahin, A. S. B. Tan, *ChemistrySelect* **5** (2020) 9730 (https://doi.org/10.1002/slct.202001498)
6. R. Y. Sumaiya, S. A. Chhanda, A. Wasif, F. Zohora, K. Akhter, M. S. Islam, N. Uddin, M. E. Halim, *J. Mol. Struct.* **1355** (2026) 145000 (https://doi.org/10.1016/j.molstruc.2025.145000)
7. G. Yenişehirli, N. A. Öztaş, E. Şahin, M. Çelebier, N. Ancın, S. G. Öztaş, *Heteroat. Chem.* **21** (2010) 373 (https://doi.org/10.1002/hc.20628)
8. D. Pardaeva, A. Tavman, D. Gürbüz, M. Hacıoğlu, F. N. Yilmaz, O. Şahin, A.S. B. Tan, A. Çınarlı, *Rev. Roum. Chim.* **69** (2024) 83 (https://doi.org/10.33224/rrch.2024.69.1-2.10)
9. D. Pardaeva, A. Tavman, E. Erçag, M. Hacıoğlu, D. Gürbüz, A. Çınarlı, A.S. Birteksöz Tan, *Fr. Ukr. J. Chem.* **12** (2024) 92 (https://doi.org/10.17721/fujcV12I1P92-110)
10. E. Alterhoni, A. Tavman, M. Hacioglu, O. Şahin, A. S. B. Tan, *J. Mol. Struct.* **1229** (2021) 129498 (https://doi.org/10.1016/j.molstruc.2020.129498)
11. S. Y. Ebrahimipour, I. Sheikhshoaie, A. C. Kautz, M. Ameri, H. Pasban-Aliabadi, H. A. Rudbari, G. Bruno, C. Janiak, *Polyhedron* **93** (2015) 99 (https://doi.org/10.1016/j.poly.2015.03.037)
12. L. A. Alfonso-Herrera, S. Rosete-Luna, D. Hernández-Romero, J. M. Rivera-Villanueva, J. L. Olivares-Romero, J. A. Cruz-Navarro, A. Soto-Contreras, A. Arenaza-Corona, D. Morales-Morales, R. Colorado-Peralta, *ChemMedChem* **17** (2022) e202200367 (https://doi.org/10.1002/cmdc.202200367)
13. Z.-J. Zhang, H.-T. Zeng, Y. Liu, D.-Z. Kuang, F.-X. Zhang, Y.-X. Tan, W.-J. Jiang, *Inorg. Nano-Metal Chem.* **48** (2018) 486 (https://doi.org/10.1080/24701556.2019.1571513)
14. G. Sahu, E. R. Tiekink, R. Dinda, *Inorganics* **9** (2021) 66 (https://doi.org/10.3390/inorganics9090066)
15. N. Patel, A. K. Prajapati, R. N. Jadeja, R. N. Patel, S. K. Patel, I. P. Tripathi, N. Dwivedi, V. K. Gupta, R. J. Butcher, *Polyhedron* **180** (2020) 114434 (https://doi.org/10.1016/j.poly.2020.114434)
16. Y. Ma, H. Liu, C. Li, Y. Zhang, M. Lv, D. Mu, S. Yin, R. Liu, *J. Mol. Struct.* **1309** (2024) 138172 (https://doi.org/10.1016/j.molstruc.2024.138172)
17. W. Y. Zhu, K. Liu, X. Zhang, *Sens. Diagn.* **2** (2023) 665 (https://doi.org/10.1039/d3sd00020f)
18. R. Sathyanarayana, V. Kumar, G.H. Pujar, B. Poojary, M.K. Shankar, S. Yallappa, *J. Photochem. Photobiol., A* **401** (2020) 112751 (https://doi.org/10.1016/j.jphotochem.2020.112751)
19. A. Tavman, M. Hacioglu, D. Gürbüz, A. Cinarli, M. A. F. Oksüzömer, A. S. B. Tan, *Bull. Chem. Soc. Ethiop.* **33** (2019) 451 (https://doi.org/10.4314/bcse.v33i3.6)
20. A. Tavman, A. Cinarli, D. Gürbüz, A.S. Birteksöz, *J. Iran. Chem. Soc.* **9** (2012) 815 (https://doi.org/10.1007/s13738-012-0098-z)
21. A. Tavman, D. Gürbüz, A. A. Karaçelik, D. N. Çolak, D. Efe, A. Cinarli, *Rev. Roum. Chim.* **69** (2024) 201 (https://doi.org/10.33224/rrch.2023.68.10-12.07)
22. A. Tavman, A. Z. Elmal, D. Gürbüz, M. Hacioglu, A.S. Birteksöz Tan, A. Çinarli, *Rev. Roum. Chim.* **68** (2023) 49 (https://doi.org/10.33224/rrch.2023.68.1-2.05)

23. A. Tavman, D. Gürbüz, Ş. Öksüz, A. Çinarli, *Mor. J. Chem.* **6** (2018) 328 (https://revues.imist.ma/index.php/morjchem/article/view/7909/6695)
24. X. Totta, A. A. Papadopoulou, A. G. Hatzidimitriou, A. Papadopoulos, G. Psomas, *J. Inorg. Biochem.* **145** (2015) 79 (https://doi.org/10.1016/j.jinorgbio.2015.01.009)
25. A. Kerflani, K. S. Larbi, A. Rabahi, A. Bouchoucha, S. Zaater, S. Terrachet-Bouaziz, *Inorg. Chim. Acta* **529** (2022) 120659 (https://doi.org/10.1016/j.ica.2021.120659)
26. K. Griffiths, A. Tsipis, P. Kumar, O. P. E. Townrow, A. Abdul-Sada, G. R. Akien, A. Baldansuren, A. C. Spivey, G. E. Kostakis, *Inorg. Chem.* **56** (2017) 9563 (https://doi.org/10.1021/acs.inorgchem.7b01011)
27. H. Ke, W. Wei, Y.-Q. Zhang, J. Zhang, G. Xie, C. Gang, S. Chen, *Dalton Trans.* **47** (2018) 16616 (http://dx.doi.org/10.1039/C8DT03983F)
28. H. Ke, W. Wei, Y. Yang, J. Zhang, Y.-Q. Zhang, G. Xie, S. Chen, *Dalton Trans.* **48** (2019) 7844 (https://doi.org/10.1039/C9DT01074B)
29. J. Zhao, J. Ji, S. Wang, Y. Luo, Z. You, *J. Coord. Chem.* **74** (2021) 3127 (https://doi.org/10.1080/00958972.2021.2024522)
30. B. Taxak, J. Devi, B. Kumar, M. Rani, *J. Mol. Struct.* **1322** (2025) 140309 (https://doi.org/10.1016/j.molstruc.2024.140309)
31. *Chemazone online chemical service of Aurora fine chemicals*, https://chemazone.com/info?ID=136.567.528 (27 March 2026)
32. H. F. Ridley, G. W. Spickett, G. M. Timmis, *J. Het. Chem.* **2** (1965) 453 (https://doi.org/10.1002/jhet.5570020424)
33. Z. Karimi-Jaberi, M. Amir, *E-J. Chem.* **9** (2012) 167 (https://doi.org/10.1155/2012/793978)
34. O. S. Ürgüt, A. Tavman, M. G. Eser, *Chem. J. Mold.* **17** (2022) 73 (http://dx.doi.org/10.19261/cjm.2022.957)
35. M27-A3: *Clinical and Laboratory Standards Institute (CLSI)*, *Reference Method for Broth Dilution Antifungal Susceptibility Testing of Yeasts*; Approved Standard-Third Edition (2012)
36. M100-Ed.31: *Clinical and Laboratory Standards Institute (CLSI), Performance Standards for Antimicrobial Susceptibility Testing* (2021)
37. K. Fukushima, T. Takahashi, M. Takaguchi, H. Ueyama, S. Ito, Y. Kurebayashi, T. Kawanishi, J. L. McKimm-Breschkin, T. Takimoto, A. Minami, T. Suzuki. *Biol. Pharm. Bull.* **34** (2011) 996 (https://doi.org/10.1248/bpb.34.996)
38. G. M. Sheldrick, *Acta Cryst., A* **64** (2008) 112 (https://doi.org/10.1107/S0108767307043930)
39. G. M. Sheldrick, *Acta Cryst., C* **71** (2015) 3 (https://doi.org/10.1107/S2053229614024218)
40. *APEX2*, Bruker AXS Inc., Madison, WI, 2013
41. C. F. Macrae, I. J. Bruno, J. A. Chisholm, P. R. Edgington, P. McCabe, E. Pidcock, L. Rodriguez-Monge, R. Taylor, J. van de Streek, P. A. Wood, *J. Appl. Cryst.* **41** (2008) 466 (https://doi.org/10.1107/S0021889807067908)
42. L. J. Farrugia, *J. Appl. Cryst.* **45** (2012) 849 (https://doi.org/10.1107/S0021889812029111)
43. D. Lomjanský, C. Rajnák, J. Titis, J. Monco, L. Smolko, R. Boča, *Inorg. Chim. Acta* **483** (2018) 352 (https://doi.org/10.1016/j.ica.2018.08.029)
44. A. G. Starikov, R. M. Minyaev, V. I. Minkin, *Chem. Phys. Lett.* **459** (2008) 27 (https://doi.org/10.1016/j.cplett.2008.04.132)
45. A. J. Bridgeman, *Dalton Trans.* **2008** (2008) 1989 (https://doi.org/10.1039/B717767D)

46. E. Kwaskowska-Chec, M. Kubiak, T. Glowiak, J.J. Ziolkowski, *Transit. Met. Chem.* **23** (1998) 641 (https://doi.org/10.1023/A:1006909528805)
47. D. L. Reger, A. E. Pascui, E. A. Foley, M. D. Smith, J. Jezierska, A. Wojciechowska, S. A. Stoian, A. Ozarowski, *Inorg. Chem.* **56** (2017) 2884 (https://doi.org/10.1021/acs.inorgchem.6b02933)
48. W. Geary, *Coord. Chem. Rev.* **7** (1971) 81 (https://doi.org/10.1016/S0010-8545(00)80009-0)
49. R. Singh, A. Prakash, S. K. Dhiman, B. Balagurumurthy, A. K. Arora, S. K. Puri, T. Bhaskar, *Bioresour. Technol.* **165** (2014) 319 (https://doi.org/10.1016/j.biortech.2014.02.076)
50. E. Kaki, A. Altındal, B. Salih, Ö. Bekaroglu, *Dalton Trans.* **44** (2015) 8293 (https://doi.org/10.1039/C5DT00540J)
51. L. J. Duarte, R. E. Bruns, *J. Phys. Chem., A* **122** (2018) 9833 (https://doi.org/10.1021/acs.jpca.8b09141)
52. K. I. Hadjiivanov, D. A. Panayotov, M. Y. Mihaylov, E. Z. Ivanova, K. K. Chakarova, S. M. Andonova, N. L. Drechev, *Chem. Rev.* **121** (2021) 1286 (https://doi.org/10.1021/acs.chemrev.0c00487)
53. Y. Kaya, H. Mutlu, G. Irez, *Gazi Univ. J. Sci.* **23** (2010) 13 (https://dergipark.org.tr/en/download/article-file/82956)
54. H. G. Bheemanna, V. Gayathri, N. M. N. Gowda, *IOSR-J. App. Chem.* **7** (2014) 17 (https://doi.org/10.9790/5736-07421722)
55. S. Tripathi, A. Dey, M. Shanmugam, R. S. Narayanan, V. Chandrasekhar, in *Organometallic Magnets. Topics in Organometallic Chemistry*, V. Chandrasekhar, F. Pointillart, Eds., Springer, Cham, 2018 (https://doi.org/10.1007/3418_2018_8)
56. J. Meletiadis, J.F. Meis, J.W. Mouton, J.P. Donnelly, P.E. Verweij, *J. Clin. Microbiol.* **38** (2000) 2949 (https://doi.org/10.1128/jcm.38.8.2949-2954.2000).

Journal of the Serbian Chemical Society
JSCS-info@shd.org.rs • www.shd.org.rs/JSCS
J. Serb. Chem. Soc. 91 (0) S1–S26 (2026) *Supplementary material*

SUPPLEMENTARY MATERIAL TO

Metal complexes with Schiff base and benzimidazolylphenol ligands with *tert*-butyl and methoxy groups: Structural characterization and biological evaluation

DILDORA PARDAEVA[1], AYDIN TAVMAN[2]*, MAYRAM HACIOGLU[3], ONUR ŞAHIN[4], MEHMET ALTUN[5] and AYŞE SEHER BIRTEKSÖZ TAN[3]

[1]Istanbul University-Cerrahpaşa, Institute of Graduate Education, Department of Chemistry, 34320, Avcilar, Istanbul, Türkiye, [2]Istanbul University-Cerrahpaşa, Faculty of Engineering, Department of Chemistry, Inorganic Chemistry Division, 34320, Avcilar, Istanbul, Türkiye, [3]Istanbul University, Faculty of Pharmacy, Department of Pharmaceutical Microbiology, 34452, Beyazit, Istanbul, Türkiye, [4]Sinop University, Faculty of Health Sciences, Department of Occupational Health and Safety, 57000 Sinop, Türkiye and [5]Istanbul University-Cerrahpaşa, Faculty of Engineering, Department of Chemistry, Organic Chemistry Division, 34320, Avcilar, Istanbul,Türkiye

J. Serb. Chem. Soc. 91 (0) (2026) 000–000

4-tert-*Butyl-2-{[(*E*)-(2-hydroxy-3-methoxyphenyl)methylidene]amino}phenol* (***H*$_2$*L*^{1}**). Decomposition point (Dec. p.): 138 °C. (+)ESI-MS (*m/z*): calculated for $[C_{18}H_{21}NO_3]^+$ 299.4, observed 297.3 (90.6 %) ($[C_{18}H_{21}NO_3$ - 2H$]^+$ and 300.4 for ($[C_{18}H_{21}NO_3$ + H$]^+$ (64.1 %). Combustion analysis for $C_{18}H_{21}NO_3$: Calculated C 72.22, H 7.07, N 4.68; found C 72.41, H 7.11, N 4.60. FT-IR (ATR, cm^{-1}): 3509m,br ν(NH), 3054w ν(CH)$_{ar.}$, 2958m ν(CH)$_{al.}$, 1630m ν(C=N), 1619m ν(C=C), 1498m, 1455m, 1351m, 1289m, 1225m ν(C–O), 1204m ν(C–O), 1070s, 831m δ(CH)$_{ar.}$, 740m, 623m, 572m, 465m, 425m. ^{1}H NMR (500 MHz, DMSO-d$_6$, δ / ppm): 9.57 (*s*, 1H, OH1), 9.00 (*s*, 1H, N=CH), 7.36 (*d*, 1H, *J* = 2.4, H3), 7.21 (*dd*, 1H, J_1 = 7.9, J_2 = 1.4, H6'), 7.14 (*dd*, 1H, J_1 = 8.5, J_2 = 2.4, H5), 7.06 (*dd*, 1H, J_1 = 8.0, J_2 = 1.4, H4'), 6.89 (*d*, 1H, *J* = 8.5, H6), 6.84 (*t*, 1H, J_1 = 7.9, J_2 = 7.9, H5'), 3.81 (*s*, 3H, OCH$_3$), 1.28 (*s*, 9H, –C(CH$_3$)$_3$). ^{13}C NMR (125 MHz, DMSO-d$_6$, δ / ppm): 161.6 (N=CH), 152.5 (C–OH(2')), 149.0 (C–OCH$_3$), 148.6 (C–OH(1')), 142.5 (C–C(CH$_3$)), 134.0 (C2), 125.2 (C5), 124.3 (C6'), 119.7 (C3), 118.2 (C6), 116.7 (C1'), 116.5 (C5'), 115.5 (C4'), 56.3 (OCH$_3$), 34.4 (–C(CH$_3$)$_3$). 31.8 (–C(CH$_3$)$_3$). UV-vis spectra (DMSO, λ_{max} / nm): 315m,br, 348m,br, 456w,br.

2-(5-*tert*-Butyl-1*H*-benzimidazol-2-yl)-6-methoxyphenol (**HL^2**): Dec.p.: 219 °C. (+)ESI-MS (*m/z*): calculated for $[C_{18}H_{20}N_2O_2]^+$ 296.4, observed 297.3 (100 %) ($[C_{18}H_{20}N_2O_2$ - H$]^+$ and 298.3 for ($[C_{18}H_{20}N_2O_2$ + 2H$]^+$ (20.7 %). Combustion analysis for $C_{18}H_{20}N_2O_2$: Calculated C 72.95, H 6.80, N 9.45; found C 73.07, H 6.91, N 9.30. FT-IR (ATR, cm^{-1}): 3351m ν(NH+OH), 3072w ν(CH)$_{ar}$, 2960m ν(CH)$_{al}$, 1619m ν(C=N), 1604m ν(C=C), 1576m, 1462m, 1364m, 1254s ν(C–O), 1202m ν(C–O), 1059m, 972m, 808m δ(CH)$_{ar}$,, 785m, 732m, 655m, 557m, 511m, 457m, 425m. ^{1}H NMR (500 MHz, DMSO-d$_6$, δ / ppm): 13.12 (*s,br*, 2H, NH+OH),

* Corresponding author. E-mail: atavman@iuc.edu.tr

7.59 (*dd*, 1H, J_1 = 8.0, J_2 = 1.3, H6), 7.55 (*s,br*, 2H, H4+H6'), 7.36 (*dd*, 1H, J_1 = 8.5, J_2 = 1.5 Hz, H4'), 7.06 (*dd*, 1H, J_1 = 8.0, J_2 = 1.2, H7), 6.93 (*t*, 1H, J_1 = 8.0, J_2 = 8.0, H5'), 3.81 (*s*, 3H, OCH_3), 1.35 (*s*, 9H, $–C(CH_3)_3$). ^{13}C NMR (125 MHz, DMSO-d_6, δ / ppm): 161.4 (C2), 152.7 ($\underline{C}–OCH_3$), 149.6 ($\underline{C}–$OH), 145.6 ($\underline{C}–C(CH_3)$), 132.2 (C9), 131.3 (C8), 122.0 (C3'), 121.1 (C4'), 120.7 (C6), 120.1 (C2'), 117.1 (C7), 113.9 (C4), 109.3 (C5'), 56.2 (OCH_3), 34.5 ($–\underline{C}(CH_3)_3$), 31.7 ($–C(\underline{C}H_3)_3$). UV-vis spectra (DMSO, λ_{max} / nm): 304m, 316m, 330m,br, 382m,br. Fluorescence spectra (EtOH, $c = 1\times10^{-4}$ mol L^{-1}, λ_{max} / nm): 463m.

[Co(**L^1**)(H_2O)$_2$]·H_2O (**1a**): Brown solid. Yield: 67 %. Dec. p.: 167 °C. Combustion analysis for $C_{18}H_{25}NO_6Co$ (FW: 410.33): Calculated C 52.69, H 6.14, N 3.41; found C 52.40, H 5.84, N 3.28. Magnetic moment, μ_{eff}: 4.06 μ_B. Λ_M (DMF, 25 °C, S m^2 mol^{-1}): 21.4. FT-IR (ATR, cm^{-1}): 3223m,br ν(OH), 3062w,br ν(CH)$_{ar}$, 2957m ν(CH)$_{al}$, 1646m ν(C=N), 1611m ν(C=C), 1565m, 1490m, 1440m, 1362m, 1257s ν(C–O), 1225m, 1096m, 1050m, 957m, 822m δ(CH)$_{ar}$, 723m, 684m ν(N→M), 541m ν(O→M), 495m, 452m. TGA (t / °C: weight loss, %): 50: 0.3; 75: 1.5; 100: 4.6 (1 mole of H_2O); 150: 7.8; 200: 9.5 (1 mole of H_2O); 250: 12.3; 300: 18.3; 350: 36.5; 400: 47.8; 450: 58.0; 500: 67.5; 550: 80.1; 600: 80.1; 650: 80.1; 700: 80.2 (Theoretical value of CoO: 18.3 %). UV-vis spectra (DMSO, λ_{max} / nm): 227w, 253m, 278m,br, 354m, 464m,br.

[Ni(**L^1**)(H_2O)$_2$] (**1b**): Greenish brown solid. Yield: 70 %. Dec. p.: 186 °C. Combustion analysis for $C_{18}H_{23}NO_5Ni$ (FW: 392.07): Calculated C 55.14, H 5.91, N 3.57; found C 55.33, H 6.06, N 3.51. Magnetic moment, μ_{eff}: 2.04 μ_B. Λ_M (DMF, 25 °C, S m^2 mol^{-1}): 21.4. FT-IR (ATR, cm^{-1}): 3065w,br ν(CH)$_{ar}$, 2957m ν(CH)$_{al}$, 1633sh ν(C=N), 1615m ν(C=C), 1506m, 1440m, 1362m, 1245m ν(C–O), 1222s, 1129m, 1078m, 975m, 820m δ(CH)$_{ar}$, 732s, 682m ν(N→M), 587m, 536m ν(O→M), 496m, 454m, 425m. TGA (t / °C: weight loss, %): 50: 0.2; 75: 0.3; 100: 0.4; 150: 3.1; 200: 12.3 (2 mole of H_2O); 250: 15.5; 300: 22.1; 350: 27.2; 400: 60.1; 450: 78.9; 500: 80.0; 550: 80.0; 600: 80.0; 650: 80.0; 700: 80.0 (Theoretical value of NiO: 19.1 %). UV-vis spectra (DMSO, λ_{max} / nm): 232w, 255m, 300m,br, 343m,br, 356sh, 440m,br.

[Cu(**L^1**)(H_2O)] (**1c**): Brown solid. Yield: 73 %. Dec. p.: 295 °C. Combustion analysis for $C_{18}H_{21}NO_4Cu$ (FW: 378.9): Calculated C 57.69, H 4.36, N 2.64; found C 57.43, H 4.21, N 2.49. Magnetic moment, μ_{eff}: 1.72 μ_B. Λ_M (DMF, 25 °C, S m^2 mol^{-1}): 32.0. FT-IR (ATR, cm^{-1}): 3346m,br ν(OH), 3080w,br ν(CH)$_{ar}$, 2962m ν(CH)$_{al}$, 1647m ν(C=N), 1612m ν(C=C), 1588m, 1506m, 1463m, 1351m, 1258m ν(C–O), 1093m, 1027m, 821m δ(CH)$_{ar}$, 781m, 731m, 688m ν(N→M), 584m, 537m ν(O→M), 477m, 422m. TGA (t / °C: weight loss, %): 50: 0.1; 75: 0.4; 100: 0.6; 150: 4.4; 200: 5.0 (1 mole of H_2O); 250: 10.5; 300: 29.8; 350: 45.1; 400: 47.0; 450: 59.7; 500: 68.0; 550: 79.2; 600: 79.4; 650: 79.9; 700: 79.9 (Theoretical value of CuO: 21.0 %). UV-vis spectra (DMSO, λ_{max} / nm): 242w, 254m, 272m,br, 307sh, 363m,br, 478w,br.

[Zn(**L^1**)(H_2O)]·H_2O (**1d**): Dark yellow solid. Yield: 65 %. Dec. p.: 173 °C. Combustion analysis for $C_{18}H_{23}NO_5Zn$ (FW: 398.8): Calculated C 49.79, H 5.34, N 3.23; found C 49.90, H 5.20, N 3.11. Λ_M (DMF, 25 °C, S m^2 mol^{-1}): 23.4. FT-IR (ATR, cm^{-1}): 3336m,br ν(OH), 3211m,br, 3061w,br ν(CH)$_{ar}$, 2957m ν(CH)$_{al}$, 1637m ν(C=N), 1615m ν(C=C), 1506m, 1435m, 1363m, 1285m, 1234m ν(C–O), 1195m ν(C–O), 1022m, 875m, 819m δ(CH)$_{ar}$, 734m, 684m ν(N→M), 586m, 537m ν(O→M), 497m, 415m. ^{1}H NMR (500 MHz, DMSO-d_6, δ / ppm): 8.86 (*s*, 1H, N=CH), 7.50 (*s,br*, 1H, *J* = 2.4, H3), 7.19 (*d*, 1H, *J* = 7.1, H6'), 7.03 (*s,br*, 1H, H5), 6.88 (*s,br*, 1H, H4'), 6.78 (*d,br*, 1H, *J* = 6.8, H6), 6.38 (*t*, 1H, J_1 =7.7, J_2 = 7.8, H5'), 3.75 (s, 3H, OCH_3), 1.27 (*s*, 9H, $–C(CH_3)_3$). ^{13}C NMR (125 MHz, DMSO-d_6, δ / ppm): 164.8 (N=CH), 161.3 (C–OH2), 152.7 ($\underline{C}–OCH_3$), 144.8 (C–OH1'), 142.4 ($\underline{C}–C(CH_3)$), 130.1 (C2), 127.3 (C5), 123.8 (C6'), 119.4 (C3), 117.1 (C6), 114.3 (C1'), 111.5 (C5'), 107.6 (C4'), 55.0 (OCH_3), 32.2 ($–\underline{C}(CH_3)_3$), 29.5 ($–C(\underline{C}H_3)_3$). TGA (t / °C: weight loss, %): 50: 1.1; 75: 2.5; 100: 4.6 (1 mole of

H_2O); 150: 4.4; 200: 9.5 (1 mole of H_2O); 250: 12.2; 300: 23.1; 350: 29.5; 400: 33.0; 450: 63.0; 500: 78.6; 550: 78.8; 600: 78.9; 650: 79.0; 700: 79.0 (Theoretical value of ZnO: 20.4%). UV-vis spectra (DMSO, λ_{max} / nm): 228 w, 253 w, 279 m, 354 m,br, 464 m,br.

K[Pd(**L**^{1})Cl]·H_2O (**1e**): Light brown solid. Yield: 77 %, Dec. p.: 265 °C. Combustion analysis for $C_{18}H_{21}ClNO_4KPd$ (FW: 496.3): Calculated C 43.56, H 4.26, N 2.82; found C 43.70, H 4.11, 2.68. Λ_M (DMF, 25 °C, S m^2 mol^{-1}): 83.2. FT-IR (ATR, cm^{-1}): 3036m,br ν(CH)$_{ar}$, 2958m ν(CH)$_{al}$, 1646m ν(C=N), 1611m ν(C=C), 1506m, 1456m, 1351m, 1289m, 1257s ν(C–O), 1204m ν(C–O), 1097m, 1024m, 965m, 912m, 826m δ(CH)$_{ar}$, 730m, 673m ν(N→M), 564m, 540m ν(O→M), 500m, 462m. ^{1}H-NMR (500 MHz, DMSO-d$_6$, δ / ppm): 8.64 (*s*, 1H, N=CH), 7.94 (*d*, 1H, J=3.0, H3), 7.43 (*d*, 1H, J=8.1 H6'), 7.30 (*d*, 1H, J=8.5, H5), 7.09 (*d*, 1H, *J* = 8.2, H4'), 7.02 (*d*, 1H, *J* = 8.6, H6), 6.72 (*t*, 1H, J_1 = 8.7, J_2 = 8.5, H5'), 3.72 (*s*, 3H, OCH_3), 1.30 (*s*, 9H, –C(CH$_3$)$_3$). ^{13}C NMR (125 MHz, DMSO-d$_6$, δ / ppm): 174.3 (N=CH), 161.5 (C–OH2), 148.4 (C–OCH$_3$), 146.9 (C–OH1'), 139.5 (C–C(CH$_3$)), 134.3 (C2), 126.3 (C5), 125.3 (C6'), 118.4 (C3), 118.3 (C6), 115.2 (C1'), 113.6 (C5'), 112.5 (C4'), 55.9 (OCH_3), 35.7 (–C(CH$_3$)$_3$), 32.1 (–C(CH$_3$)$_3$). TGA (t / °C: weight loss, %): 50: 0.7; 75: 2.0; 100: 3.7 (1 mole of H_2O); 150: 3.9; 200: 4.1; 250: 4.3; 300: 6.0; 350: 7.5; 400: 20.0; 450: 67.0; 500: 74.7; 550: 75.3; 600: 75.6; 650: 75.9; 700: 76.0 (Theoretical value of PdO: 24.6 %). UV-vis spectra (DMSO, λ_{max} / nm): 233w, 255m, 309sh, 318m,br, 337sh, 430m,br, 451sh.

[Co(**L**^{2})Cl(H_2O)] (**2a**): Dark brown solid. Yield: 72 %. Dec. p.: 201 °C. Combustion analysis for $C_{18}H_{21}ClN_2O_3Co$ (FW: 407.8): Calculated C 53.02, H 5.19, N 6.87; found C 54.10, H 5.00, N 6.72. Magnetic moment, μ_{eff}: 2.17 μ_B. Λ_M (DMF, 25 °C, S m^2 mol^{-1}): 35.4. FT-IR (ATR, cm^{-1}): 3198m,br ν(OH), 3088m,br ν(CH)$_{ar}$, 2960m ν(CH)$_{al}$, 1606m ν(C=N), 1573m ν(C=C), 1463m, 1435m, 1361m, 1244s ν(C–O), 1195m, 1060m, 981m, 813m δ(CH)$_{ar}$, 786m, 732s, 66 m ν(N→M), 601m, 574m, 545m ν(O→M), 501m, 470m, 420m. TGA (t / °C: weight loss, %): 50: 0.1; 75: 0.2; 100: 0.4; 150: 3.1; 200: 5.2 (1 mole of H_2O); 250: 9.9; 300: 29.0; 350: 66.0; 400: 67.1; 450: 68.2; 500: 69.4; 550: 82.4; 600: 82.5; 650: 82.6; 700: 82.6 (Theoretical value of CoO: 18.4 %). UV-vis spectra (DMSO, λ_{max} / nm): 240w, 253w, 307m,br, 320m,br, 334sh, 473w,br. Fluorescence spectra (EtOH, $c = 1\times10^{-4}$ mol L^{-1}, λ_{max} / nm): 425sh, 451m,br.

[Ni(**L**^{2})Cl(H_2O)]·H_2O (**2b**): Light brown solid. Yield: 70 %. Dec. p.: 198 °C. Combustion analysis for $C_{18}H_{23}ClN_2O_4Ni$ (FW: 425.5): Calculated C 50.81, H 5.45, N 6.58; found C 50.90, H 5.51, N 6.43. Magnetic moment, μ_{eff}: 2.05 μ_B. Λ_M (DMF, 25 °C, S m^2 mol^{-1}): 38.8. FT-IR (ATR, cm^{-1}): 3373m,br ν(OH), 3228m,br, 3070m,br ν(CH)$_{ar}$, 2962m ν(CH)$_{al}$, 2872m, 1611m ν(C=N), 1598m ν(C=C), 1545m, 1440m, 1362m, 1249m ν(C–O), 1198m ν(C–O), 1015m, 983m, 863m, 814m δ(CH)$_{ar}$, 731m, 671m ν(N→M), 581m, 540m ν(O→M), 457m, 420m. TGA (t / °C: weight loss, %): 50: 0.3; 75: 2.2; 100: 4.6 (1 mole of H_2O); 150: 7.8; 200: 9.0 (1 mole of H_2O); 250: 19.3; 300: 22.8; 350: 24.4; 400: 36.9; 450: 53.0; 500: 65.1; 550: 72.1; 600: 75.3; 650: 82.6; 700: 83.0 (Theoretical value of NiO: 17.5 %). UV-vis spectra (DMSO, λ_{max} / nm): 241w, 253w, 309m,br, 357m,br, 373m,br, 461m,br. Fluorescence spectra (EtOH, $c = 1\times10^{-4}$ mol L^{-1}, λ_{max} / nm): 399w, 478m.

[Cu(**L**^{2})Cl] (**2c**): Brown solid. Yield: 76 %. Dec. p.: 235 °C. Combustion analysis for $C_{18}H_{19}ClN_2O_2Cu$ (FW: 394.4): Calculated C 54.82, H 4.86, N 7.10; found C 55.90, H 5.05, N 6.92. Magnetic moment, μ_{eff}: 1.01 μ_B. Λ_M (DMF, 25 °C, S m^2 mol^{-1}): 48.8. FT-IR (ATR, cm^{-1}): 3215m,br ν(OH), 3057w,br ν(CH)$_{ar}$, 2962m ν(CH)$_{al}$, 1608m ν(C=N), 1589m ν(C=C), 1543m, 1485m, 1384m, 1242s ν(C–O), 1199m ν(C–O), 1062m, 981m, 815m δ(CH)$_{ar}$, 786m, 732s, 667m ν(N→M), 576m, 543m ν(O→M), 470m, 418m. TGA (t / °C: weight loss, %): 50: 0.2; 75: 0.3; 100: 0.4; 150: 0.5; 200: 1.6; 250: 4.2; 300: 6.4; 350: 13.4; 400: 26.5; 450: 43.0; 500: 65.0; 550: 76.0; 600: 78.1; 650: 80.0; 700: 81.0 (Theoretical value of CuO: 20.2 %). UV-

vis spectra (DMSO, λ_{max} / nm): 243w, 255m, 297sh, 307m, 321m, 335m,br, 371sh, 433m,br. Fluorescence spectra (EtOH, $c = 1\times10^{-4}$ mol L^{-1}, λ_{max} / nm): 404w,br, 461sh.

[Zn(**L**^{2})Cl(H_2O)]·H_2O (**2d**): Dark yellow solid. Yield: 65 %, Dec. p.: 229 °C. Combustion analysis for $C_{18}H_{23}ClN_2O_4Zn$ (FW: 432.3): Calculated C 50.02, H 5.36, N 6.48; found C 50.30, H 5.44, N 6.34. Λ_M (DMF, 25 °C, S m^2 mol^{-1}): 38.6. FT-IR (ATR, cm^{-1}): 3406m,br ν(OH), 3215m,br ν(NH), 3059w,br ν$(CH)_{ar}$, 2962m ν$(CH)_{al}$, 1614m ν(C=N), 1591m ν(C=C), 1554m, 1467m, 1386m, 1249s ν(C–O), 1199m ν(C–O), 1109m, 1078m, 975m, 852m, 825m δ$(CH)_{ar}$, 732s, 669m ν(N→M), 601m, 543m ν(O→M), 439m, 410m. ^{1}H NMR (500 MHz, DMSO-d_6, δ / ppm): 13.64 (*s,br*, 1H, NH), 7.65 (*dd,br*, 1H, $J_1 = 8.6$, $J_2 = 1.7$, H6), 7.37 (*d,br*, 2H, $J = 8.9$, H4+H6'), 7.05 (*s,br*, 1H, H4'), 6.95 (*d,br*, 1H, $J = 7.9$, H7), 6.89 (*t,br*, 1H, $J_1 = 8.0$, $J_2 = 8.1$, H5'), 3.82 (*s*, 3H, OCH_3), 1.36 (*s*, 9H, –$C(CH_3)_3$). ^{13}C NMR (125 MHz, DMSO-d_6, δ / ppm): 167.9 (C2), 159.0 (C–OCH_3), 131.9, 104.7, 54.2 (OCH_3), 32.8 (–$C(CH_3)_3$). TGA (t / °C: weight loss, %): 50: 1.9; 75: 4.1; 100: 4.3 (1 mole of H_2O); 150: 8.4; 200: 9.0 (1 mole of H_2O); 250: 21.7; 300: 34.3; 350: 75.6; 400: 80.9; 450: 81.1; 500: 81.5; 550: 81.6; 600: 81.8; 650: 82.0; 700: 82.1 (Theoretical value of ZnO: 18.8 %). UV-vis spectra (DMSO, λ_{max} / nm): 237w, 254w, 296sh, 304m, 332sh, 354sh. Fluorescence spectra (EtOH, $c = 1\times10^{-4}$ mol L^{-1}, λ_{max} / nm): 424m,br.

[Pd(**L**^{2})Cl(H_2O)] (**2e**): Light brown solid. Yield: 77%, Dec. p.: 265. Combustion analysis for $C_{18}H_{21}ClN_2O_3Pd$ (FW: 455.2): Calculated C 47.49, H 4.65, N 6.15; found C 47.12, H 4.63, N 5.90. Λ_M (DMF, 25 °C, S m^2 mol^{-1}): 49.6. FT-IR (ATR, cm^{-1}): 3293m,br ν(OH), 3197m ν(NH), 3058w,br ν$(CH)_{ar}$, 2958m ν$(CH)_{al}$, 2866m, 1602m ν(C=N), 1592m ν(C=C), 1561m, 1492m, 1436m, 1364m, 1242s ν(C–O), 1182m ν(C–O), 1075m, 981m, 812m δ$(CH)_{ar}$, 733m, 669m ν(N→M), 599m, 543m ν(O→M), 465m, 441m. ^{1}H NMR (500 MHz, DMSO-d_6, δ / ppm): 13.22 (*s,br*, 1H, NH), 8.02 (*d*, 1H, $J = 9.1$, H6), 7.61 (*d,br*, 1H, $J = 2.8$, H4), 7.39 (*d,br*, 1H, $J = 8.8$, H6'), 7.30 (*dd*, 1H, $J_1 = 8.4$, $J_2 = 1.8$, H4'), 7.23 (*dd*, 1H, $J_1 = 8.6$, $J_2 = 1.6$, H7), 6.96 (*t*, 1H, $J_1 = 8.3$, $J_2 = 7.9$, H5'), 3.84 (*s*, 3H, OCH_3), 1.39 (*s*, 9H, –$C(CH_3)_3$). ^{13}C NMR (125 MHz, DMSO-d_6, δ / ppm): 170.8 (C2), 166.2 (C–OCH_3), 159.8 (C–OH), 158.0 (C–$C(CH_3)$), 140.4, 139.3, 132.5, 119.0, 116.1, 56.2 (OCH_3), 33.2 (–$C(CH_3)_3$). TGA (t / °C: weight loss, %): 50: 0.2; 75: 0.5; 100: 0.6; 150: 3.3; 200: 5.1 (1 mole of H_2O); 250: 7.5; 300: 15.0; 350: 23.0; 400: 28.5; 450: 32.5; 500: 35.2; 550: 44.2; 600: 68.2; 650: 74.1; 700: 74.2 (Theoretical value of PdO: 26.8 %). UV-vis spectra (DMSO, λ_{max} / nm): 233m, 255m, 308m,br, 321m,br, 335m,br, 458m,br. Fluorescence spectra (EtOH, $c = 1\times10^{-4}$ mol L^{-1}, λ_{max} / nm): 393w, 472m,br.

TABLE S-I. Crystal data and structure refinement parameters for **H_2L^1**

Empirical formula	$C_{18}H_{21}NO_3$
Formula weight	299.36
Crystal system	Orthorhombic
Space group	*Pbca*
a (Å)	14.2349 (10)
b (Å)	9.5415 (5)
c (Å)	24.1061 (16)
α, β, γ (°)	90
V (Å^3)	3274.1(4)
Z	8
D_c (g cm^{-3})	1.215
μ (mm^{-1})	0.082
θ range (°)	2.5-25.2

Measured refls.	46454
Independent refls.	3898
R_{int}	0.062
S	1.04
R1/wR2	0.059/0.154
$\Delta\rho_{max}/\Delta\rho_{min}$ (eÅ^{-3})	0.19/-0.21
CCDC	2298000

TABLE S-II. Selected bond distances and angles for $\mathbf{H_2L^1}$ (Å, º)

C8—N1	1.305(3)	C3—C2—O2	125.58(19)
C1—O1	1.289(2)	C13—C15—C18	110.40(19)
C2—O2	1.364(2)	C13—C15—C17	111.9(2)
C6—C8	1.407(3)	C16—C15—C13	108.3(2)
C7—O2	1.420(3)	O3—C10—C11	125.82(19)
C9—C14	1.384(3)	O3—C10—C9	116.1(2)
C9—C10	1.396(3)	C14—C9—N1	123.33(18)
C9—N1	1.414(3)	C10—C9—N1	115.90(18)
C10—O3	1.353(3)	C8—N1—C9	127.13(19)
O1—C1—C6	122.17 (19)	N1—C8—C6	123.8(2)
O1—C1—C2	121.55 (18)	C2—O2—C7	117.37(17)
O2—C2—C1	113.32 (17)		

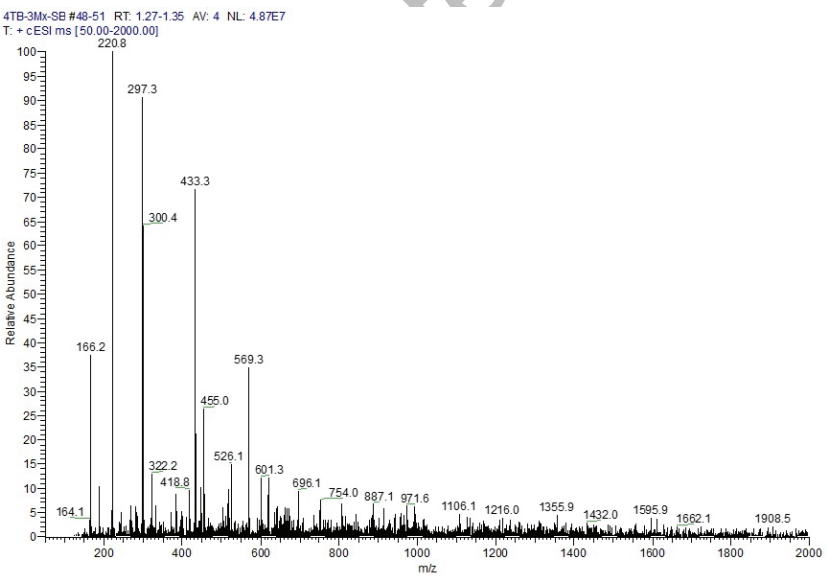

Fig. S1. ESI-MS spectrum of $\mathbf{H_2L^1}$

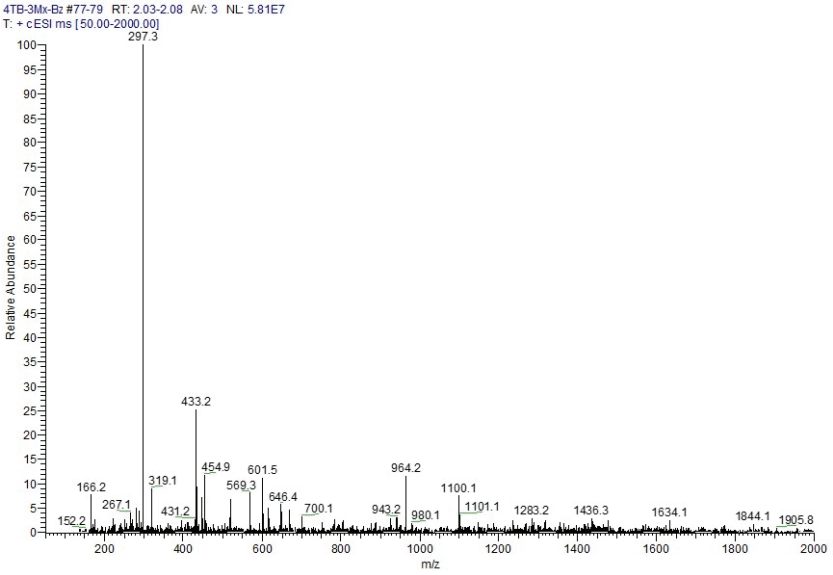

Fig. S2. ESI-MS spectrum of **HL²**

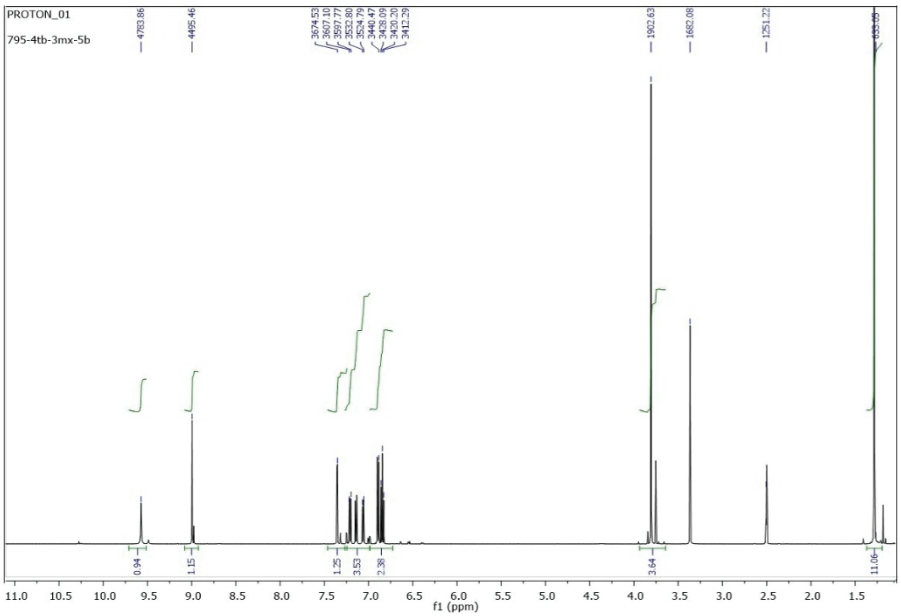

Fig. S3. ^{1}H-NMR spectrum of $\mathbf{H_2L^1}$

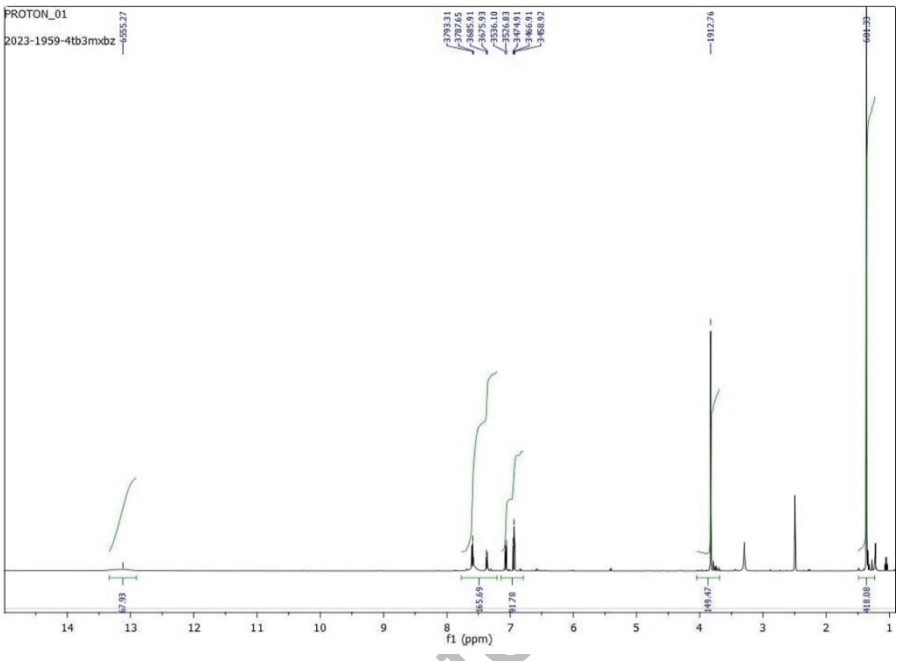

Fig. S4. ^{1}H-NMR spectrum of **HL^{2}**

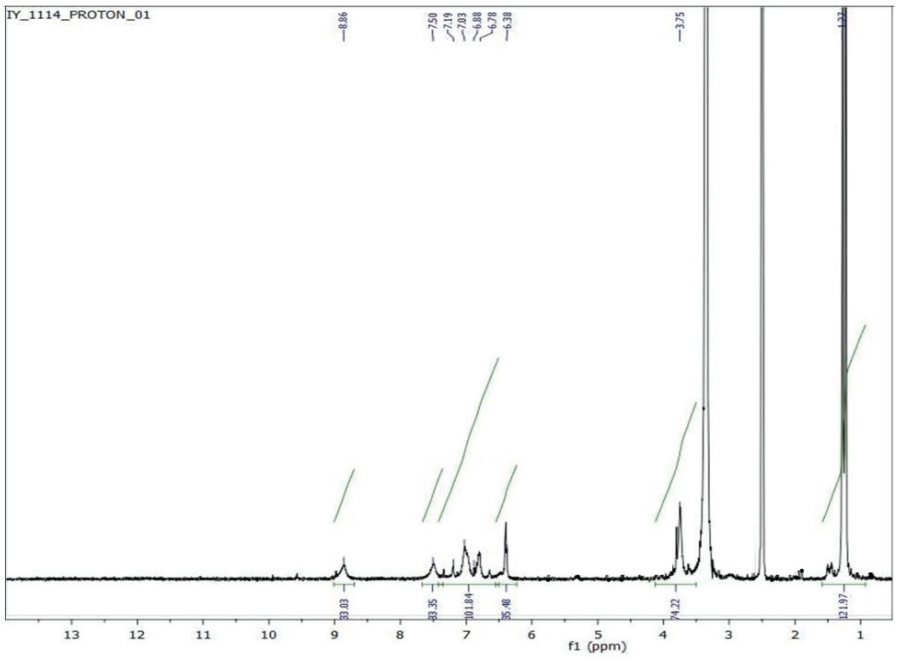

Fig. S5. ^{1}H-NMR spectrum of **1d** (Zn(II) complex of **H_2L^1**)

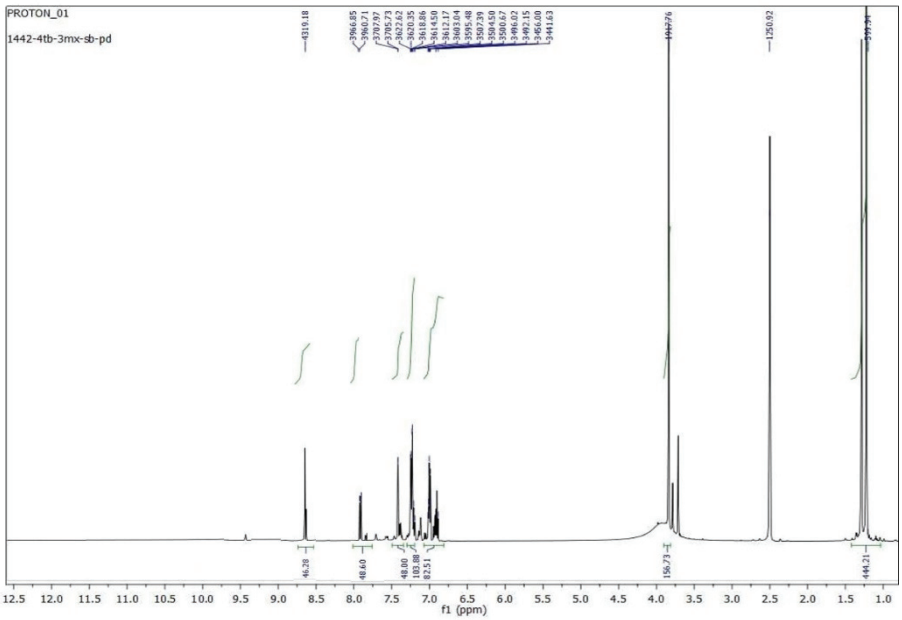

Fig. S6. ^{1}H-NMR spectrum of **1e** (Pd(II) complex of $\mathbf{H_2L^1}$)

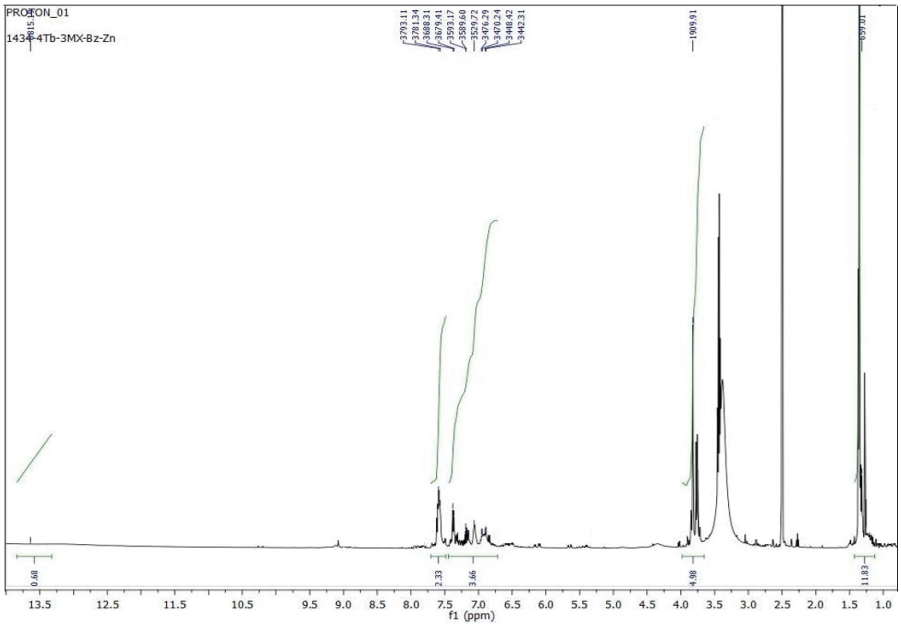

Fig. S7. ^{1}H-NMR spectrum of **2d** (Zn(II) complex of $\mathbf{HL^2}$)

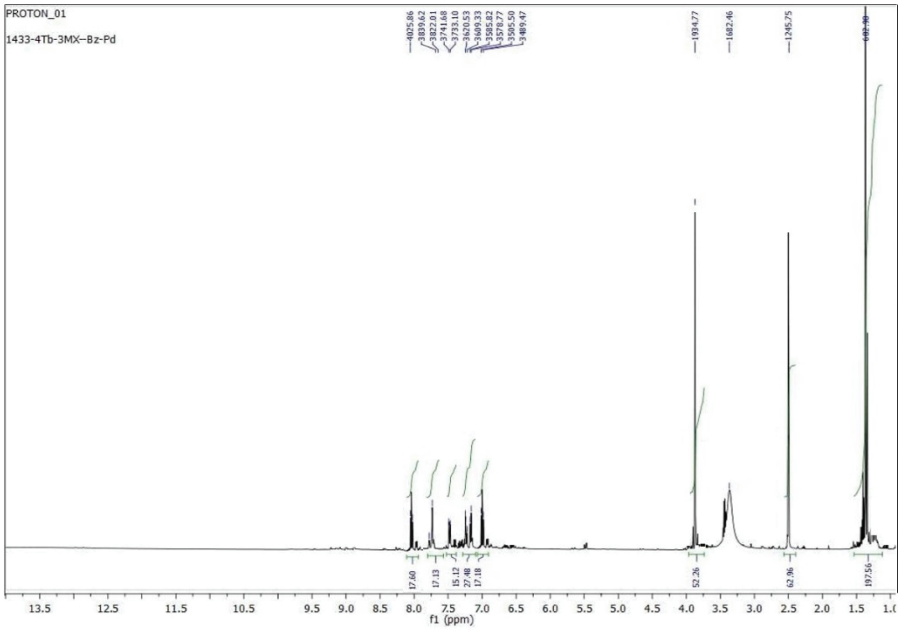

Fig. S8. ^{1}H-NMR spectrum of **2e** (Pd(II) complex of **HL^{2}**)

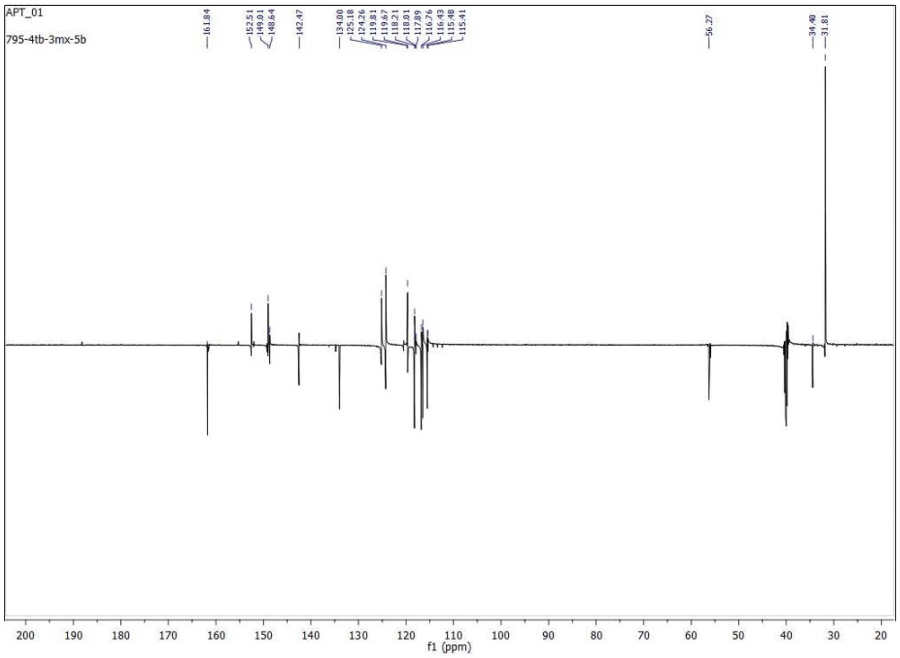

Fig. S9. ^{13}C-NMR spectrum of **H_2L^1**

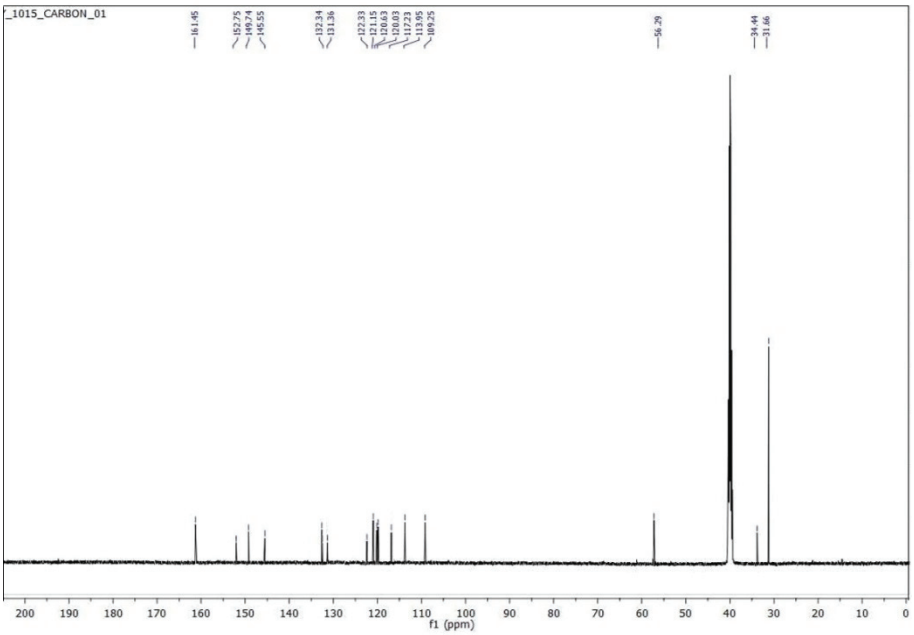

Fig. S10. ^{13}C-NMR spectrum of **HL^2**

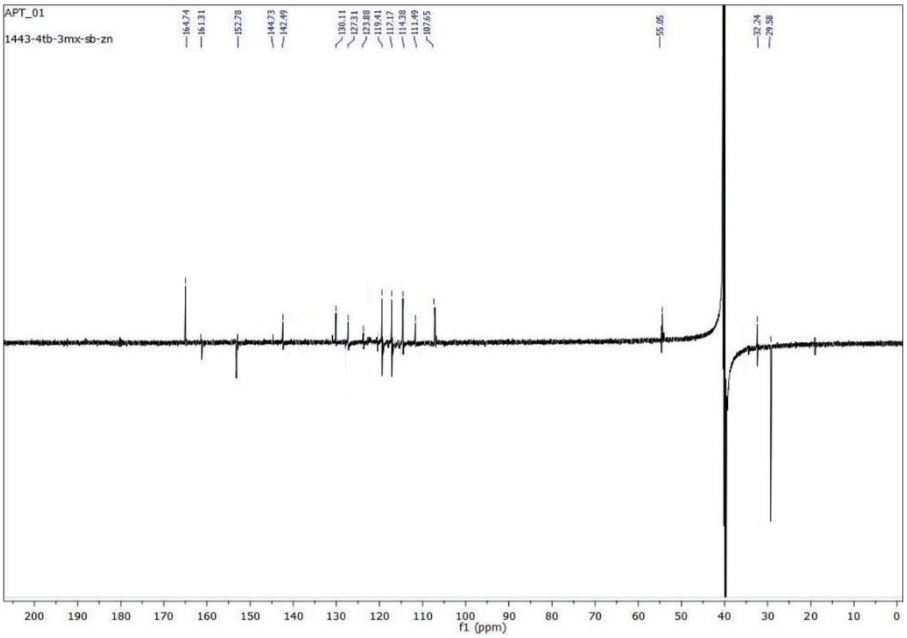

Fig. S11. ^{13}C-NMR spectrum of **1d** (Zn(II) complex of **H_2L^1**)

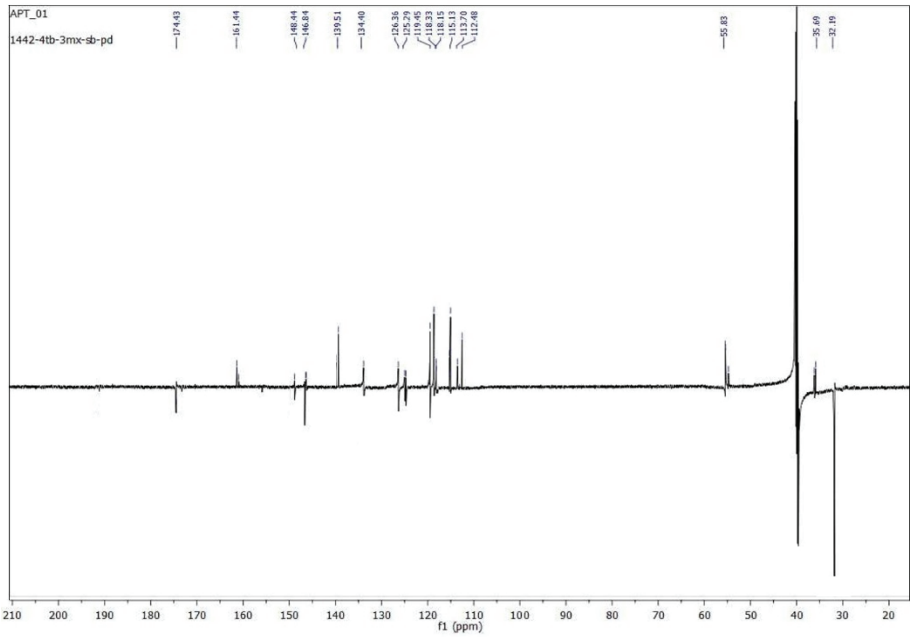

Fig. S12. ^{13}C-NMR spectrum of **1e** (Pd(II) complex of $\mathbf{H_2L^1}$)

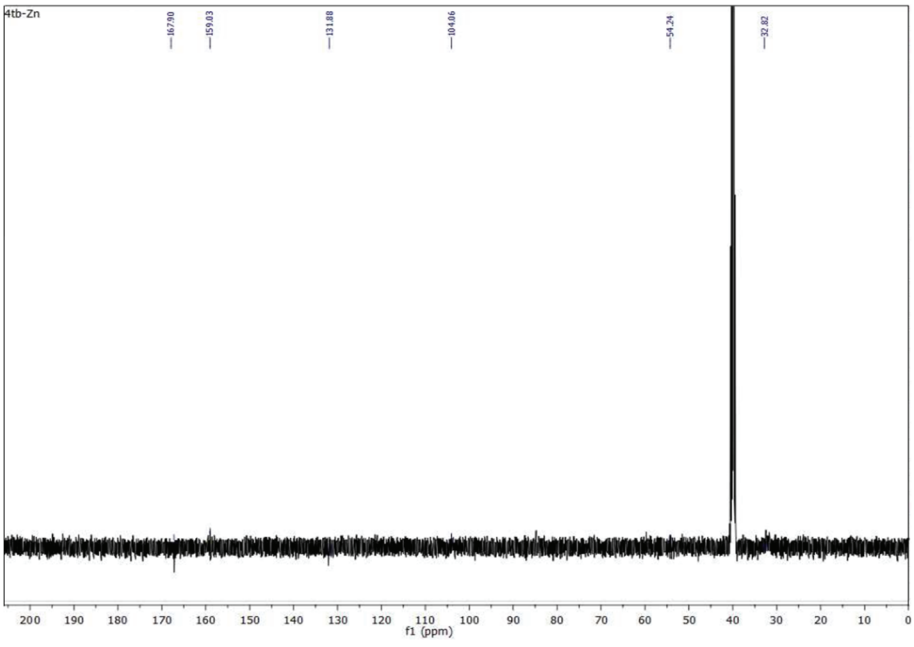

Fig. S13. ^{13}C-NMR spectrum of **2d** (Zn(II) complex of $\mathbf{HL^2}$)

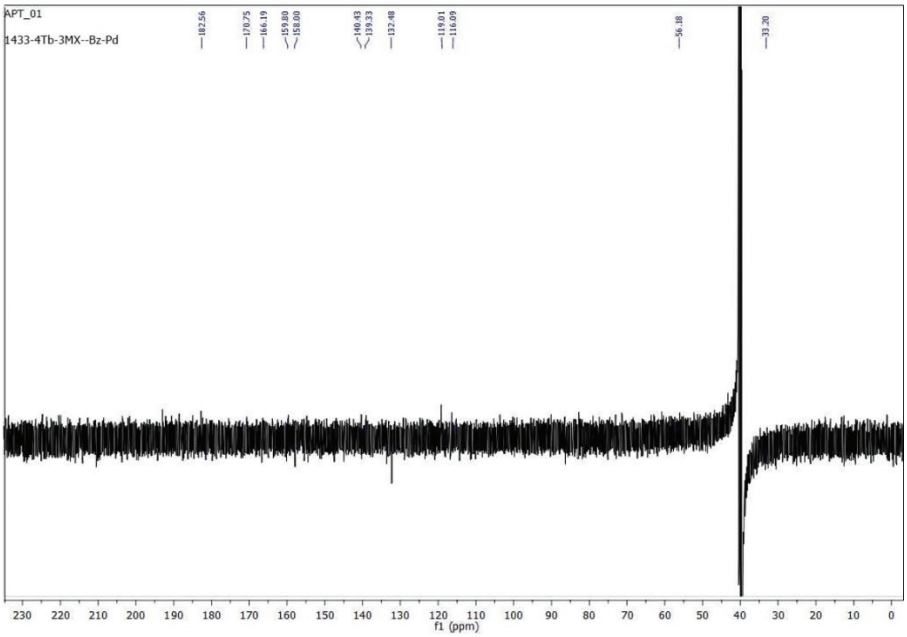

Fig. S14. ^{13}C-NMR spectrum of **2e** (Pd(II) complex of **HL^2**)

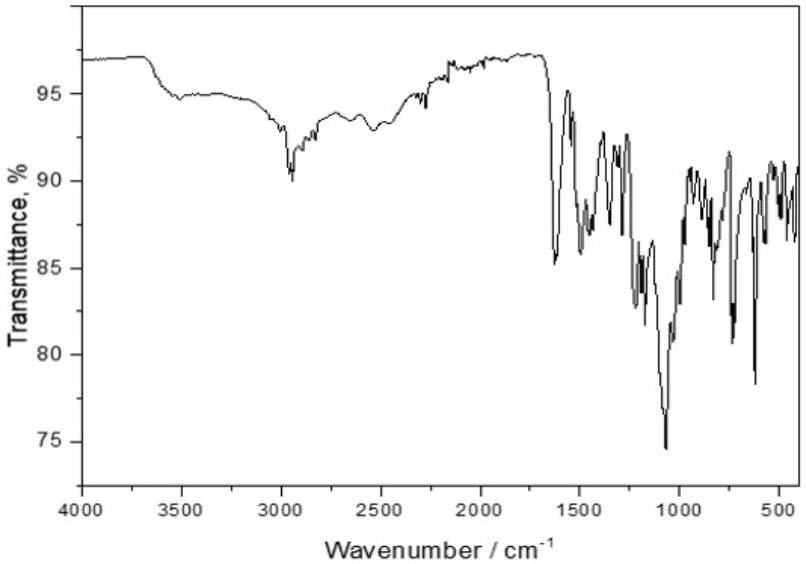

Fig. S15. FTIR spectrum of **H_2L^1**

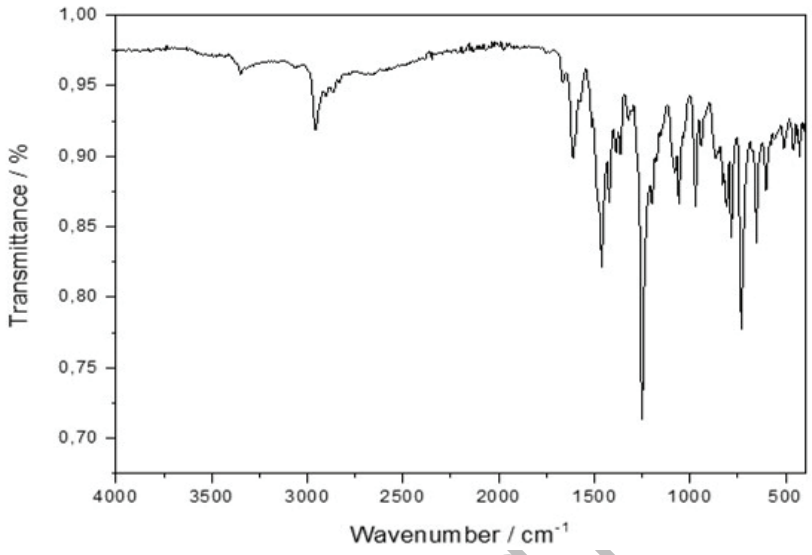

797
798 Fig. S16. FTIR spectrum of **HL²**

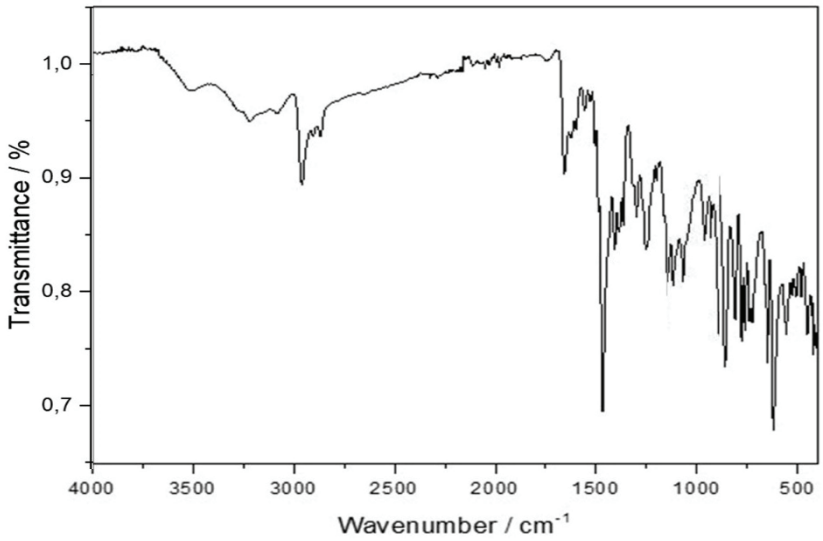

799
800 Fig. S17. FTIR spectrum of **1a**

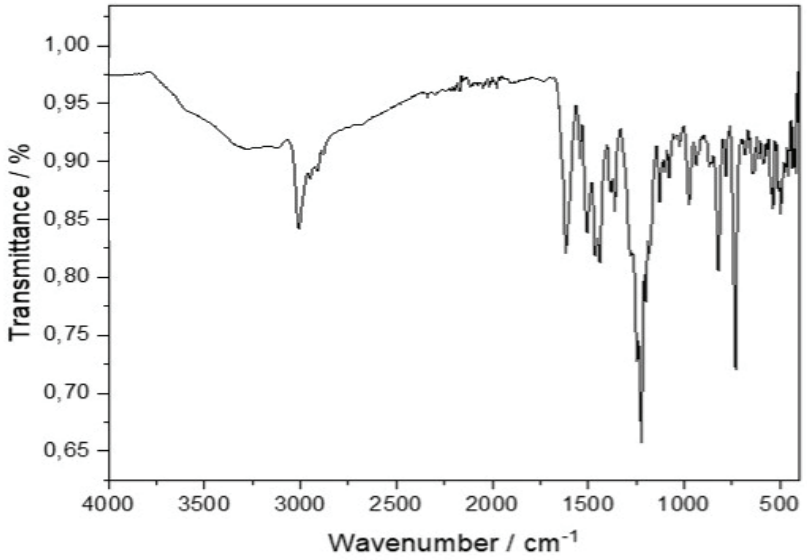

Fig. S18. FTIR spectrum of **1b**

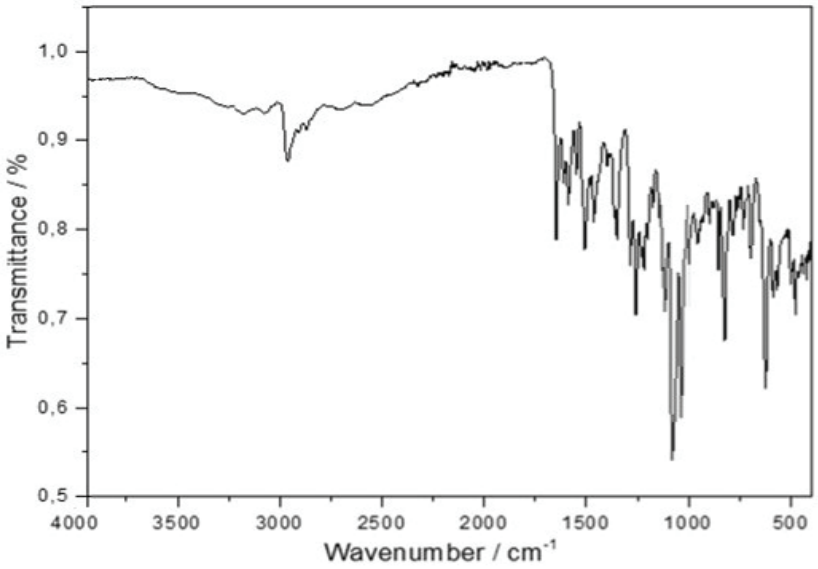

Fig. S19. FTIR spectrum of **1c**

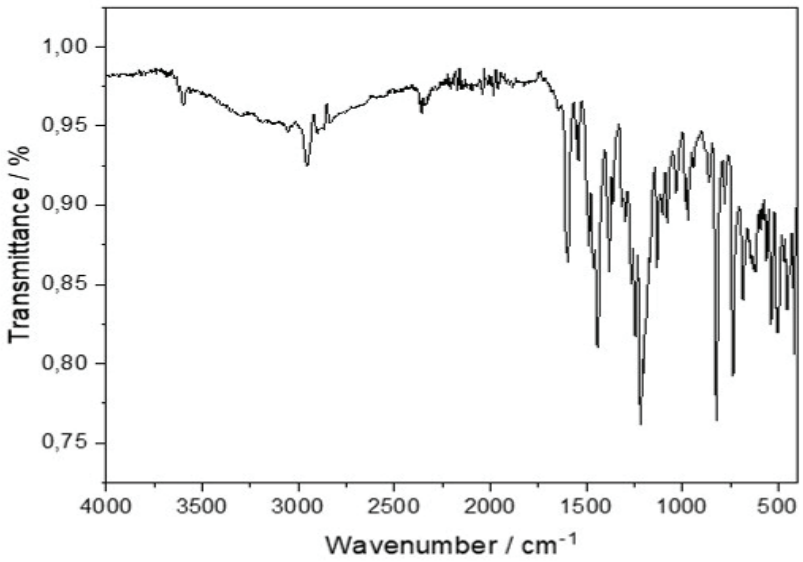

Fig. S20. FTIR spectrum of **1d**

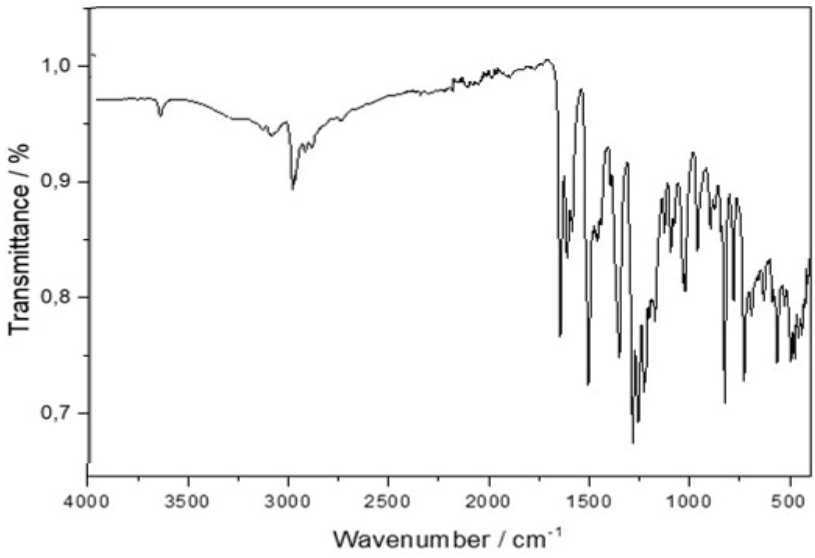

Fig. S21. FTIR spectrum of **1e**

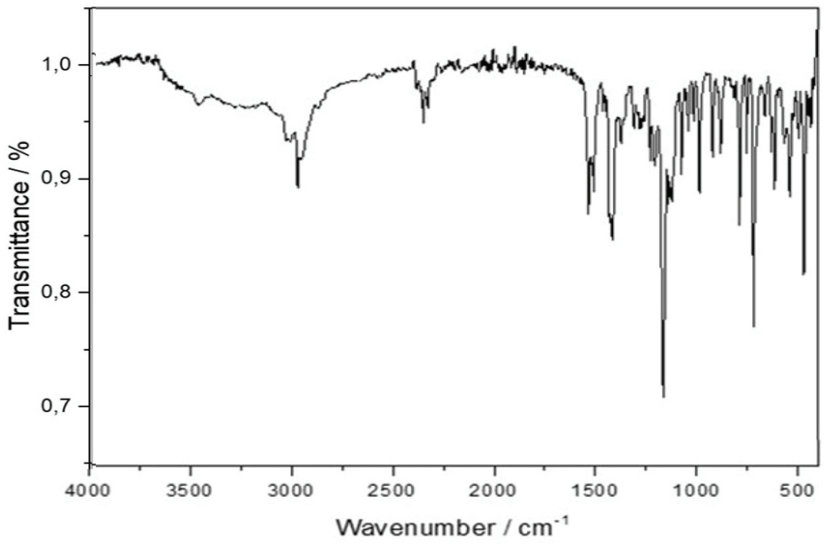

Fig. S22. FTIR spectrum of **2a**

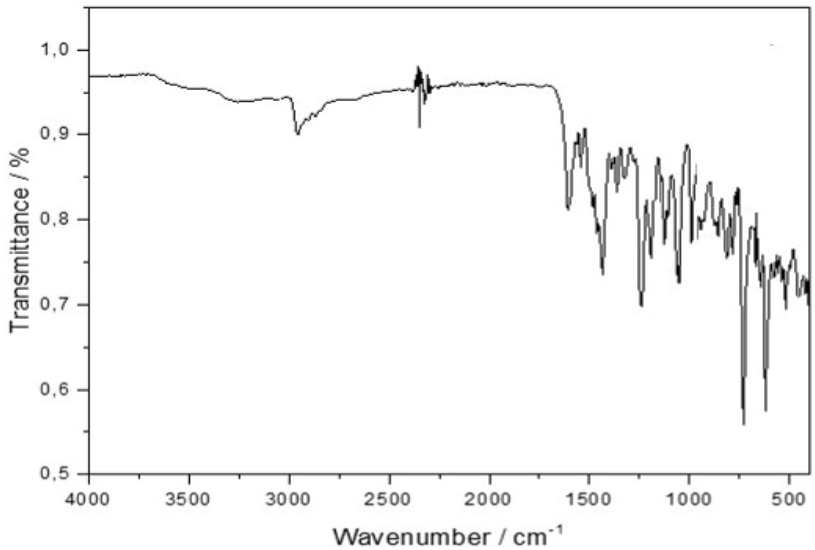

Fig. S23. FTIR spectrum of **2b**

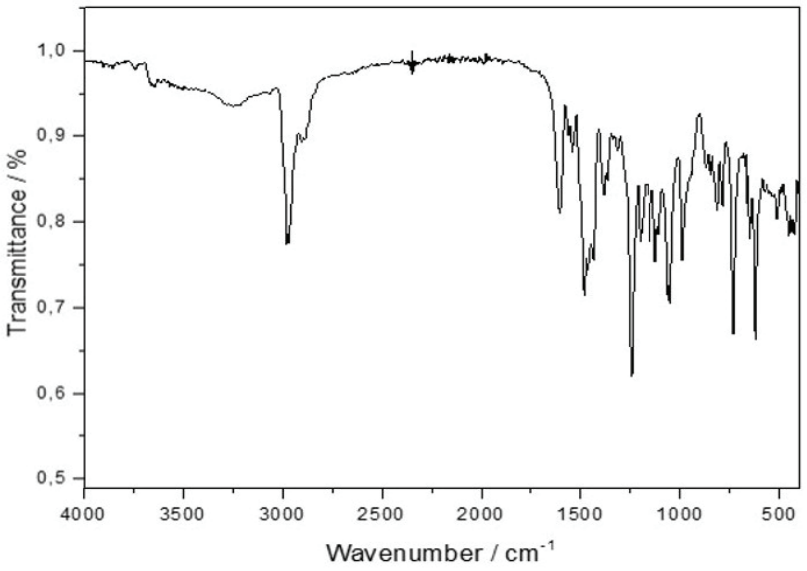

Fig. S24. FTIR spectrum of **2c**

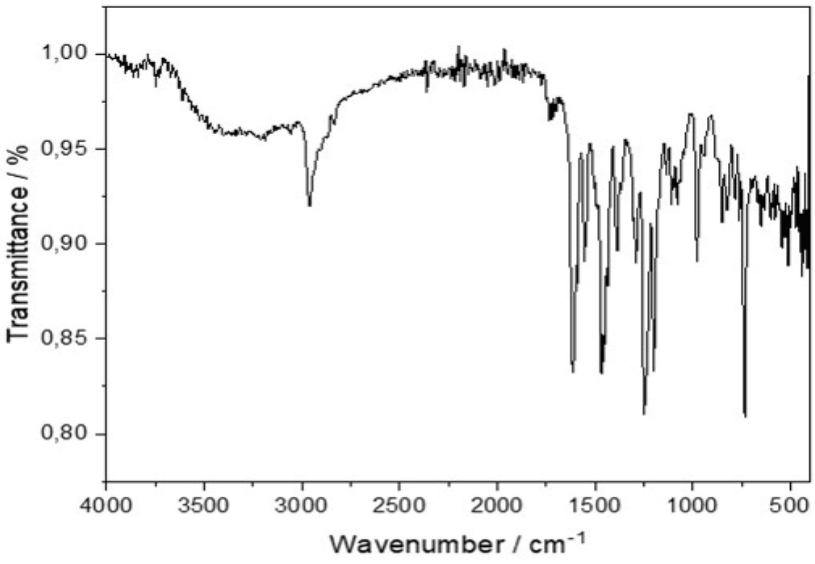

Fig. S25. FTIR spectrum of **2d**

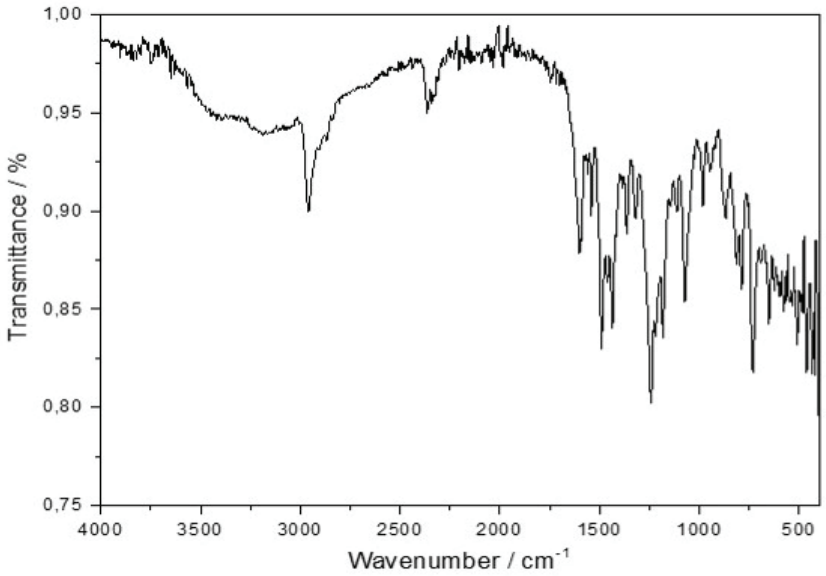

Fig. S26. FTIR spectrum of **2e**

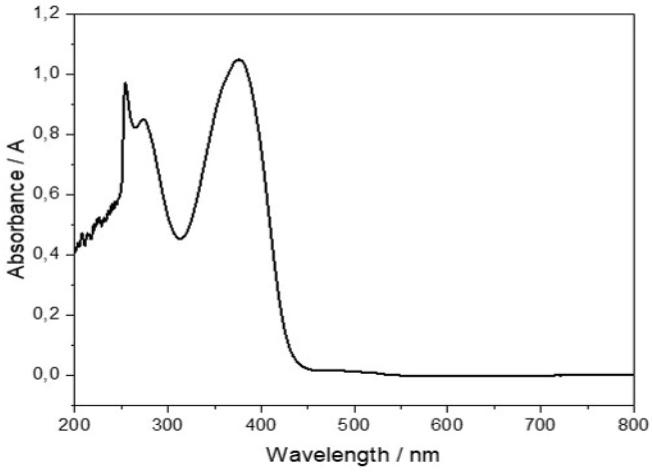

Fig. S27. UV-visible spectrum of $\mathbf{H_2L^1}$

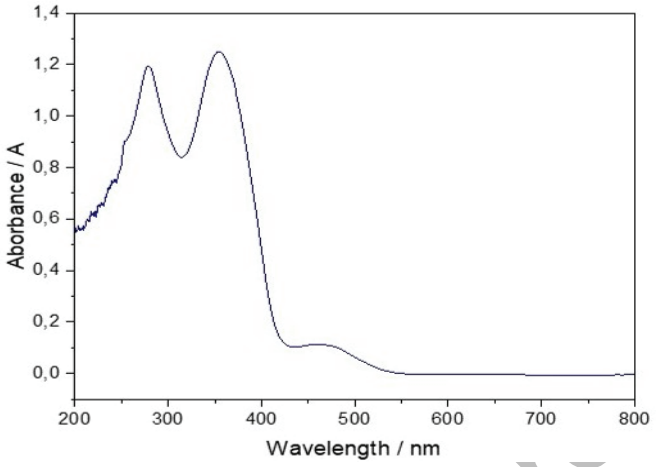

Fig. S28. UV-visible spectrum of **1a**

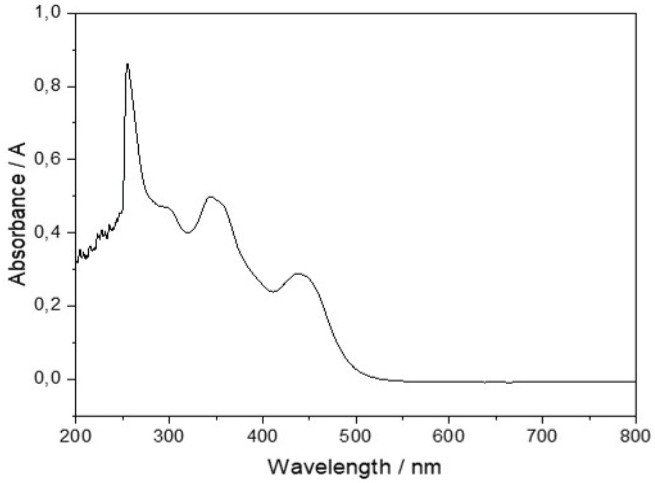

Fig. S29. UV-visible spectrum of **1b**

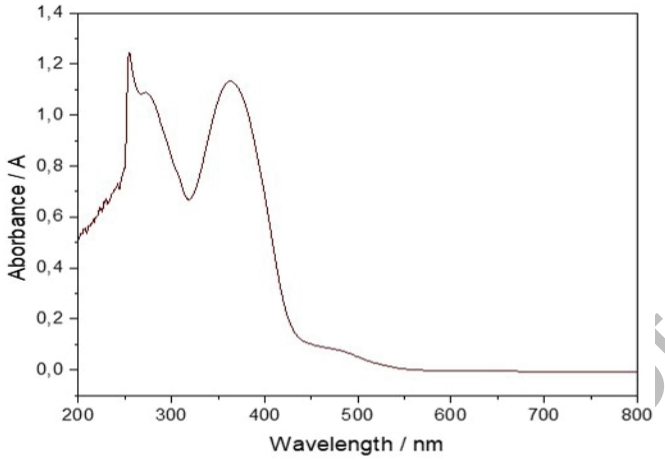

Fig. S30. UV-visible spectrum of **1c**

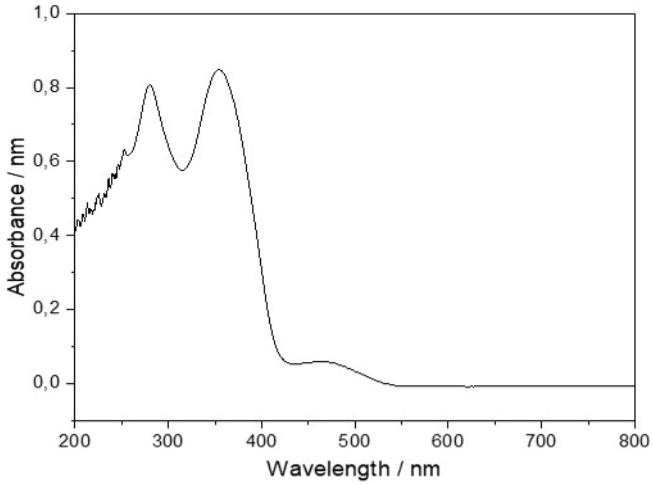

Fig. S31. UV-visible spectrum of **1d**

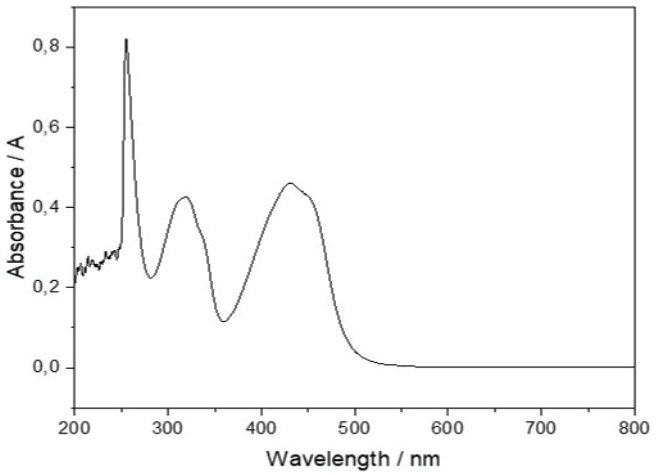

Fig. S32. UV-visible spectrum of **1e**

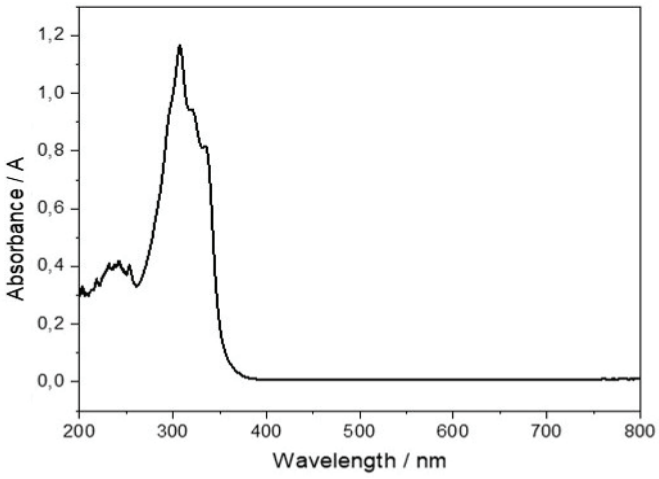

Fig. S33. UV-visible spectrum of **HL^2**

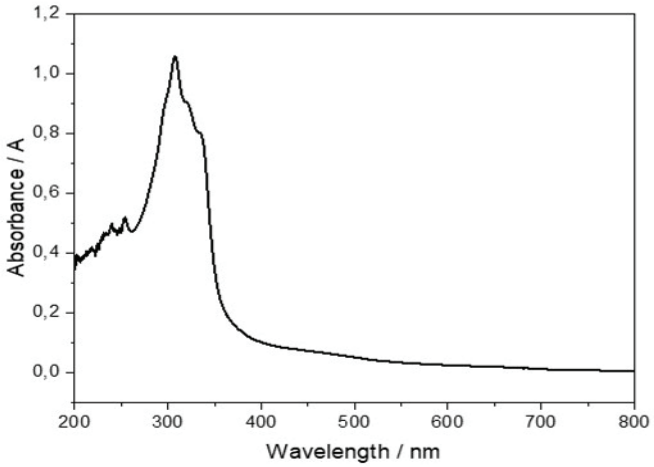

Fig. S34. UV-visible spectrum of **2a**

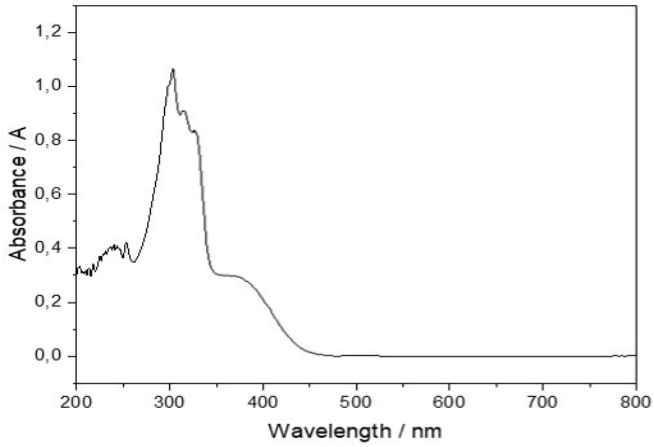

Fig. S35. UV-visible spectrum of **2b**

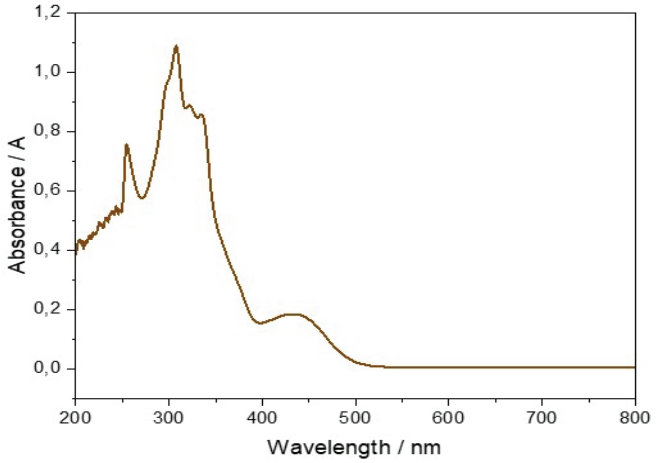

Fig. S36. UV-visible spectrum of **2c**

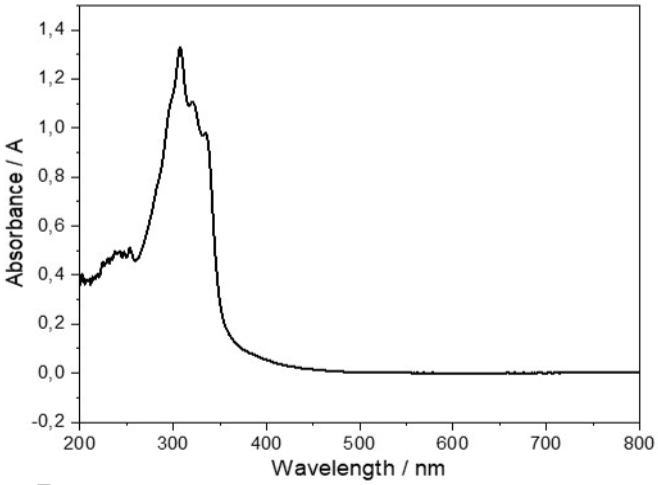

Fig. S37. UV-visible spectrum of **2d**

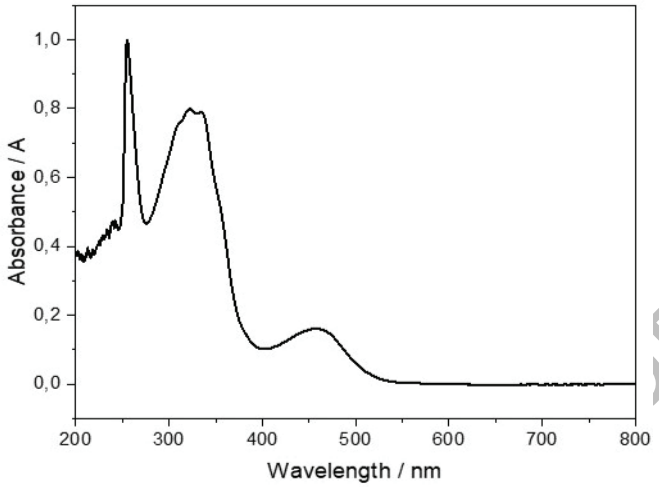

Fig. S38. UV-visible spectrum of **2e**

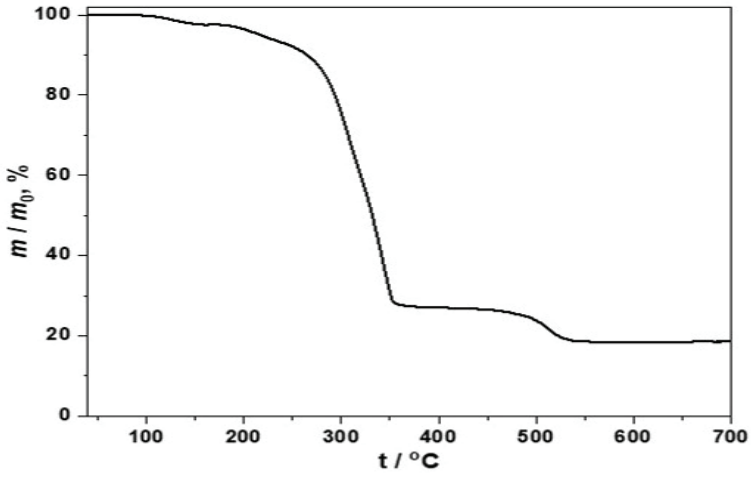

Fig. S39. TGA curve of **2a**

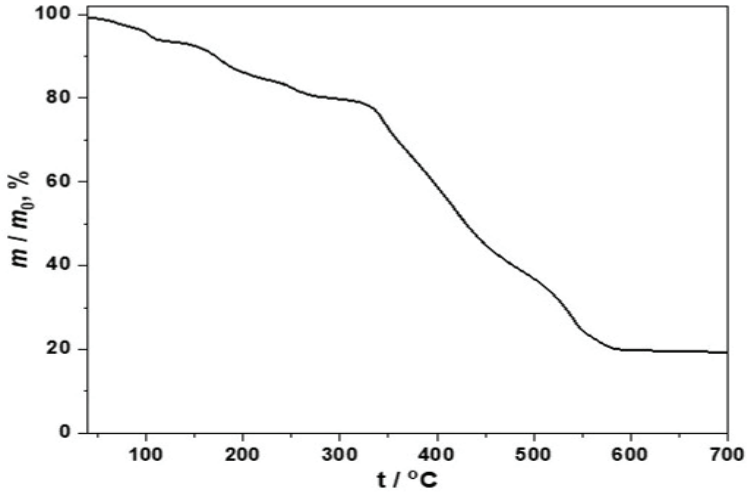

Fig. S40. TGA curve of **2b**

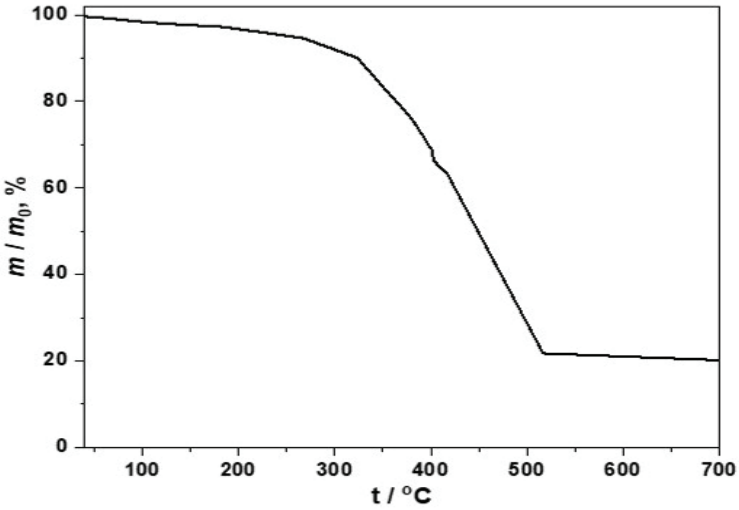

Fig. S41. TGA curve of **2c**

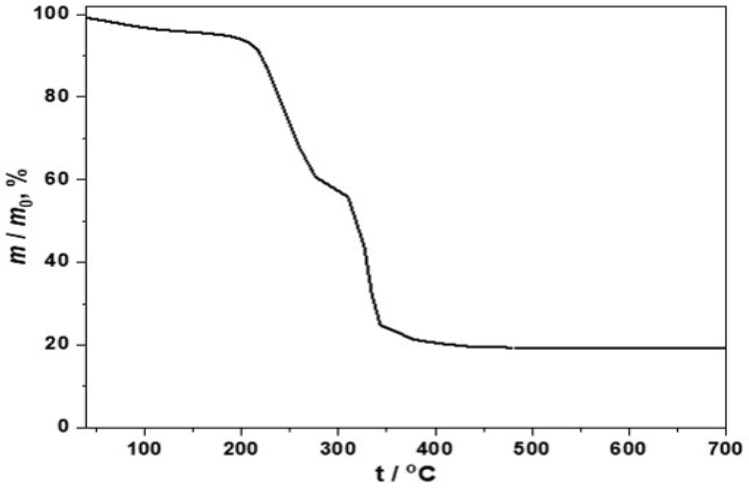

Fig. S42. TGA curve of **2d**

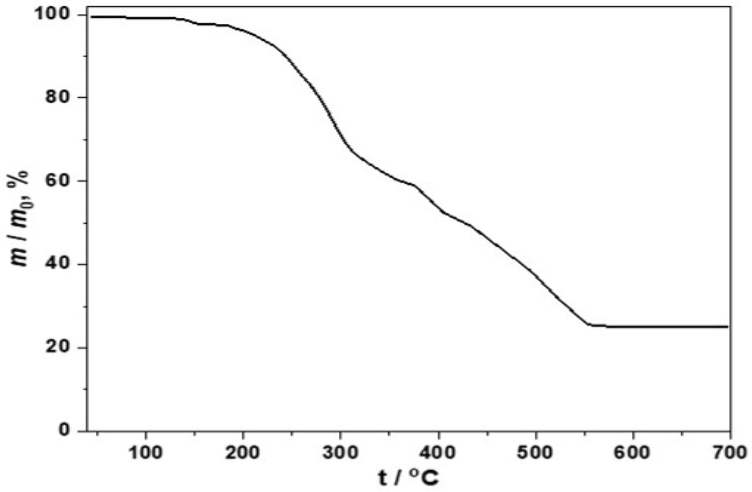

Fig. S43. TGA curve of **2e**.